### Arteriosclerosis, Thrombosis, and Vascular Biology

#### **BASIC SCIENCES**



# Cavβ3 Contributes to the Maintenance of the Blood-Brain Barrier and Alleviates Symptoms of Experimental Autoimmune Encephalomyelitis

Damian Martus, Sarah K. Williams, Kira Pichi, Stefanie Mannebach-Götz, Nicolas Kaiser, Barbara Wardas, Claudia Fecher-Trost, Markus R. Meyer, Frank Schmitz, Andreas Beck, Richard Fairless, Ricarda Diem, Veit Flockerzi, Anouar Belkacemi

**BACKGROUND:** Tight control of cytoplasmic  $Ca^{2+}$  concentration in endothelial cells is essential for the regulation of endothelial barrier function. Here, we investigated the role of  $Cav\beta 3$ , a subunit of voltage-gated  $Ca^{2+}$  (Cav) channels, in modulating  $Ca^{2+}$  signaling in brain microvascular endothelial cells (BMECs) and how this contributes to the integrity of the blood-brain barrier.

**METHODS:** We investigated the function of  $Cav\beta 3$  in BMECs by  $Ca^{2+}$  imaging and Western blot, examined the endothelial barrier function in vitro and the integrity of the blood-brain barrier in vivo, and evaluated disease course after induction of experimental autoimmune encephalomyelitis in mice using  $Cav\beta 3^{-/-}$  ( $Cav\beta 3$ -deficient) mice as controls.

**RESULTS:** We identified Cavβ3 protein in BMECs, but electrophysiological recordings did not reveal significant Cav channel activity. In vivo, blood-brain barrier integrity was reduced in the absence of Cavβ3. After induction of experimental autoimmune encephalomyelitis, Cavβ3 $^{-/-}$  mice showed earlier disease onset with exacerbated clinical disability and increased T-cell infiltration. In vitro, the transendothelial resistance of Cavβ3 $^{-/-}$  BMEC monolayers was lower than that of wild-type BMEC monolayers, and the organization of the junctional protein ZO-1 (zona occludens-1) was impaired. Thrombin stimulates inositol 1,4,5-trisphosphate—dependent Ca<sup>2+</sup> release, which facilitates cell contraction and enhances endothelial barrier permeability via Ca<sup>2+</sup>-dependent phosphorylation of MLC (myosin light chain). These effects were more pronounced in Cavβ3 $^{-/-}$  than in wild-type BMECs, whereas the differences were abolished in the presence of the MLCK (MLC kinase) inhibitor ML-7. Expression of *Cacnb3* cDNA in Cavβ3 $^{-/-}$  BMECs restored the wild-type phenotype. Coimmunoprecipitation and mass spectrometry demonstrated the association of Cavβ3 with inositol 1,4,5-trisphosphate receptor proteins.

**CONCLUSIONS:** Independent of its function as a subunit of Cav channels,  $Cav\beta3$  interacts with the inositol 1,4,5-trisphosphate receptor and is involved in the tight control of cytoplasmic  $Ca^{2+}$  concentration and  $Ca^{2+}$ -dependent MLC phosphorylation in BMECs, and this role of  $Cav\beta3$  in BMECs contributes to blood-brain barrier integrity and attenuates the severity of experimental autoimmune encephalomyelitis disease.

**GRAPHIC ABSTRACT:** A graphic abstract is available for this article.

Key Words: blood-brain barrier ■ calcium signaling ■ encephalomyelitis, autoimmune, experimental ■ endothelial cells ■ mice
■ microvascular permeability ■ myosin light chain kinase

ndothelial cells are components of the blood-brain barrier with brain microvascular endothelial cells (BMECs) being involved in controlling the permeability of the blood-brain barrier.<sup>1,2</sup> The barrier function of endothelial cells is reduced by proinflammatory

mediators such as thrombin.<sup>3</sup> Thrombin stimulates endothelial cell PAR-1 (protease-activated receptor 1), a G-protein-coupled receptor. Its stimulation leads to the activation of phospholipase C, resulting in the formation of diacylglycerol and inositol 1,4,5-trisphosphate (IP3).

Correspondence to: Priv-Doz Dr Anouar Belkacemi, Pharmakologisches Institut, Ruprecht-Karls-Universität Heidelberg, Im Neuenheimer Feld 366, 69120 Heidelberg, Germany. Email anouar.belkacemi@pharma.uni-heidelberg.de

Supplemental Material is available at https://www.ahajournals.org/doi/suppl/10.1161/ATVBAHA.124.321141. For Sources of Funding and Disclosures, see page 1849.

© 2024 The Authors. Arteriosclerosis, Thrombosis, and Vascular Biology is published on behalf of the American Heart Association, Inc., by Wolters Kluwer Health, Inc. This is an open access article under the terms of the Creative Commons Attribution Non-Commercial-NoDerivs License, which permits use, distribution, and reproduction in any medium, provided that the original work is properly cited, the use is noncommercial, and no modifications or adaptations are made.

Arterioscler Thromb Vasc Biol is available at www.ahajournals.org/journal/atvb

#### **Nonstandard Abbreviations and Acronyms**

bEnd.3 immortalized mouse brain endothelial cell **BMEC** brain microvascular endothelial cell Cav voltage-gated Ca2+ Cavβ3-/voltage-gated Ca<sup>2+</sup> channel β3-deficient DAPI 4',6-diamidino-2-phenylindole EAE experimental autoimmune encephalomyelitis GDF<sub>5</sub> growth differentiation factor 5 **GFP** green fluorescent protein **HRP** horseradish peroxidase IP3 inositol 1,4,5-trisphosphate **IRES** internal ribosome entry site junctional adhesion molecule-A JAM-A MLC myosin light chain **MLCK** myosin light chain kinase PAR-1 protease-activated receptor 1 PECAM1 platelet endothelial cell adhesion molecule Rho Ras homologous **ZO-1** zona occludens-1

IP3 binds to the IP3 receptor, leading to the release of Ca<sup>2+</sup> from intracellular stores, followed by a continuous influx of Ca2+ from the extracellular space via storeoperated cation channels4 and transient receptor potential channels.<sup>5,6</sup> Elevated cytoplasmic Ca<sup>2+</sup> concentration in endothelial cells activates MLCK (myosin light chain kinase), followed by MLC (myosin light chain) phosphorylation, cell contraction, endothelial gap formation, and increased endothelial permeability.7,8

A number of studies have demonstrated the existence of functional voltage-gated Ca2+ (Cav) channels in vascular endothelial cells, 9,10 which open upon depolarization of the plasma membrane, allowing Ca2+ influx from the extracellular space. Cav channels are multiprotein complexes consisting of the pore-forming subunit  $Cav\alpha 1$  and the auxiliary subunits Cav $\beta$ , Cav $\alpha$ 2 $\delta$ , and, in skeletal muscle, Cav $\gamma$ . 11–13 In particular, the Cav $\beta$  and Cav $\alpha$ 2 $\delta$  subunits contribute to the membrane localization of the ion-conducting Cava1 pore and to the gating of Cav channels.14-17

In addition to their role as Cav subunits, the  $Cav\beta$  and Cavα2δ subunits also have channel-independent functions. For example, the  $Cav\alpha2\delta1$  protein has been identified as a neuronal thrombospondin receptor,18 which contains binding sites for gabapentin and pregabalin.<sup>19</sup> Gabapentin and pregabalin are drugs that are used in the treatment of epilepsy and neuropathic pain. In addition, presynaptic  $\text{Cav}\alpha2\delta$  proteins are essential for the formation and organization of glutamatergic synapses and, as transsynaptic organizers of glutamatergic synapses, may align the synaptic active zone with the postsynaptic

#### **Highlights**

- Cavβ3 transcripts and proteins are present in primary brain microvascular endothelial cells where they function independently of voltage-gated Ca<sup>2+</sup> channel activity.
- Cavβ3 desensitizes cells to low inositol 1,4,5trisphosphate (IP3) levels by binding to the IP3 receptor (IP3R), and thereby contributes to Ca2+dependent MLC (myosin light chain) phosphorylation and endothelial barrier integrity.
- Deletion of the Cavβ3 gene Cacnb3 increased the permeability of brain microvascular endothelial cell monolayers in vitro and of the blood-brain barrier in
- The presence of Cavβ3 alleviates the symptoms of experimental autoimmune encephalomyelitis in vivo.

density. ^20,21 The Cav $\beta$  subunits Cav $\beta$ 1, Cav $\beta$ 3, and Cav $\beta$ 4 translocate to the nucleus where they influence gene expression.<sup>22-26</sup> When the electrical activity of innervated adult mouse muscle cells is impaired, the expression of a splice variant of Cav $\beta$ 1 (Cav $\beta$ 1e) is upregulated to limit the loss of muscle mass via GDF5 (growth differentiation factor 5). Overexpression of Cavβ1e in aged mice activates the GDF5 signaling pathway and counteracts age-related muscle mass loss. 25,26 In cardiomyocytes, a fraction of Cavβ2 translocates to the nucleus and regulates calpain-dependent hypertrophic signaling pathways.<sup>27</sup> Cavβ1 has been identified in T cells in the absence of functional Cav currents and may play a role in the regulation of T-cell proliferation and apoptosis.<sup>28</sup>

In fibroblasts, insulin-producing pancreatic  $\beta$ -cells, HEK293 and COS7 cells, we demonstrated that Cavβ3, but not Cavβ1, Cavβ2, or Cavβ4, acts as a brake on Ca<sup>2+</sup> release from intracellular stores by binding to the IP3 receptor without affecting Cav channel function. In cells in which the Cacnb3 gene has been deleted by gene targeting, IP3-dependent Ca2+ release from intracellular Ca<sup>2+</sup> stores is enhanced, resulting in accelerated wound healing, increased cell migration, collagen secretion, insulin release, and glucose excretion.<sup>29-33</sup>

In this work, we identified Cavβ3 transcripts and Cavβ3 protein in primary mouse BMECs. Genetic deletion of the Cacnb3 gene increased the permeability of BMEC monolayers in vitro and of the blood-brain barrier in vivo, and during experimental autoimmune encephalomyelitis (EAE), Cavβ3-/- (Cavβ3-deficient) mice developed more severe and earlier onset of EAE symptoms associated with increased T-cell infiltration into the central nervous system. In BMECs from Cavβ3<sup>-/-</sup> mice, thrombin-mediated Ca2+ release from intracellular stores and MLC phosphorylation were increased. The increased permeability of BMEC monolayers was significantly reduced in the presence of an inhibitor of MLCK but

not of Rho (Ras homologous)-dependent phosphatase, and the wild-type BMEC permeability phenotype was rescued by expression of the Cacnb3 cDNA in  $Cav\beta3^{-/-}$  cells. Our results indicate that  $Cav\beta3$ , independent of its role as a Cav channel subunit, associates with the IP3 receptor, affects thrombin-induced IP3-dependent  $Ca^{2+}$  release from intracellular stores of BMECs and thereby the permeability of BMEC monolayers, which may contribute to the integrity of the blood-brain barrier in vivo, and alleviates the clinical symptoms of EAE.

#### MATERIALS AND METHODS

#### **Data Availability**

Data that support the findings of this study are available from the corresponding author upon reasonable request. RNA-sequencing and mass spectrometry proteomics raw data have been made publicly available in the Gene Expression Omnibus under the accession number GSE268823 and the ProteomeXchange Consortium via PRIDE (Proteomics Identifications Database)<sup>34</sup> with the data set identifier PXD052822. Animals, antibodies, cDNA clones, cultured cells, and reagents are listed in the Major Resources Table in the Supplemental Material.

#### **Animals and Ethic Statements**

All experimental procedures were approved and performed in accordance with the ethic regulations and the Animal Welfare Committees of Saarland University, Saarland state, Heidelberg University and Regional Council, Karlsruhe, Germany. All efforts were made to minimize animal suffering and to reduce the number of animals used. Both males and females with matched age and sex were used, but sex difference and interaction were not determined in the study. For EAE experiments, only female mice with matched age were used in the study because this disease is a model for multiple sclerosis, which predominantly affects young females. For this reason, and that disease induction is reportedly higher in female rodents,35,36 young female mice are routinely used in EAE research. Mice were housed in a 12-hour light-dark cycle with access to standard diet and water ad libitum. The standard diet in Homburg was from ssniff Spezialitaten GmbH (V1534-300) containing grain and grain products, oil seed products, minerals, and tuber products. The standard diet in Heidelberg was from Altromin International (1310), which is a cereal-based (soy, wheat, and corn) fixed formula.

#### Histopathology and Immunolabeling

Animals were anesthetized with an overdose of ketamine and xylazine mix and transcardially perfused with PBS followed by ice-cold 4% paraformaldehyde in PBS (137 mmol/L NaCl, 2.7 mmol/L KCl, 8 mmol/L Na $_2$ HPO $_4$ , 2 mmol/L KH $_2$ PO $_4$ , pH 7.4) as described. Brains were removed and postfixed in ice-cold paraformaldehyde for 2 hours, followed by overnight incubation in 30% sucrose at 4 °C. Brains were frozen in freezing medium (optimal cutting temperature; Leica) and stored at -80 °C. Brains were sectioned (14- $\mu$ m thick) on a cryostat (Leica); sections were stored at -80 °C until usage. Spinal cords were dissected, postfixed for 24 hours in 4% ice-cold paraformaldehyde, and, following paraffin embedding,

0.5-µm-thick transverse sections were cut with a microtome (SM 2000R; Leica).

For immunolabeling of brain, cryosections were washed 3× in PBS for rehydration at room temperature and then incubated in blocking solution (5% [v/v] normal donkey serum and 0.5% [v/v] Triton X-100 in PBS) for 1 hour at room temperature. Sections were incubated in primary antibodies (chicken anti-GFP [green fluorescent protein] and goat anti-CD31 [cluster of differentiation 31]) overnight at 4 °C. On the following day, sections were washed 3× in PBS and incubated in secondary antibody (goat anti-chicken Alexa 488, donkey anti-goat Cy3 [Cyanine-3]) for 2 hours at room temperature. Sections were washed in PBS, and nuclei were stained with bisbenzimide. Sections were mounted in Fluoromount G and stored at 4 °C until imaging. Images were taken using the Zeiss AxioScan.Z1 slide scanner and the ZEN Blue software (Zeiss, Oberkochen, Germany).

Demyelination was investigated by Luxol fast blue staining and hematoxylin counterstain as described previously.<sup>38</sup> For anti-CD3 immunohistochemistry, antigen retrieval was performed by incubating spinal cord sections mounted on glass slides in heated (≈80 °C) 0.2% (v/v) citric acid solution (pH 6.0), before being left to cool. Endogenous peroxidases were blocked using 3% hydrogen peroxide, and nonspecific binding sites were blocked in the presence of a blocking solution containing 10% (v/v) normal goat serum and 2% (v/v) BSA. Sections were incubated overnight in the presence of anti-CD3 primary antibody. Thereafter, biotinylated secondary goat anti-rabbit antibody was applied for 1 hour, followed by 1-hour incubation in the ABC kit (Vector Laboratories) according to the manufacturer's instructions and subsequent development with 3,3′-diaminobenzidine tetrahydrochloride (Sigma-Aldrich).

Spinal cord images were acquired on a light microscope (Nikon Eclipse 80i; Nikon GmbH, Düsseldorf, Germany) using a 10× objective. Quantification was performed manually from 10 complete spinal cord cross sections evenly distributed throughout the spinal cord. The degree of demyelination was evaluated semiquantitatively using the following scoring system: 0.5, traces of perivascular or subpial demyelination; 1, marked perivascular or subpial demyelination; 2, confluent perivascular or subpial demyelination of half spinal cord cross section; and 4, transverse myelitis. Infiltration of CD3-positive T cells was quantified by counting CD3-positive cells per spinal cord section and normalized to the spinal cord area measured using Fiji (National Institutes of Health, Bethesda, MD).

For immunostaining of cultured cells, BMECs were seeded onto collagen-coated glass coverslips. When confluent, cells were washed 3× with PBS, fixed and permeabilized with 98% (v/v) methanol at -20 °C for 20 minutes (for ZO-1 [zona occludens-1] staining) or fixed with 4% (w/v) paraformaldehyde and permeabilized with 0.2% Triton X-100 in PBS for 15 minutes at 21 °C (for PECAM1 [platelet endothelial cell adhesion molecule] staining). Nonspecific binding sites were blocked in the presence of PBS buffer containing 0.1% Triton X-100, 1% normal donkey serum, and 3% BSA (ZO-1) or 0.2% Triton X-100 and 5% normal donkey serum (PECAM1) for 1 hour at 21 °C. Cells were then incubated for 16 hours at 4 °C in the presence of either rabbit anti-ZO-1 or goat anti-PECAM1 antibodies diluted in the respective blocking buffer. Next day, cells were washed 3× with PBS and incubated in PBS containing the respective Alexa Fluor 488-conjugated secondary anti-rabbit or anti-goat for 1 hour at 21 °C. Nuclei were stained using DAPI

(4',6-diamidino-2-phenylindole), and coverslips were mounted using Fluoromount G. Cells were imaged using Zeiss Axio Observer microscope (Zeiss, Oberkochen, Germany) equipped with an oil immersion 63×/1.4 Plan-Apochromat objective (Zeiss). The continuous staining of ZO-1 between cells was measured using the Image J software<sup>39</sup> (National Institutes of Health, Bethesda, MD) and normalized to the cell area.

#### Isolation and Culture of Primary Mouse BMECs

As described previously,40 adult (8-14 weeks old) wild-type (C57BL/6N) and Cavβ3-/- mice were euthanized by cervical dislocation, and brains were isolated. Brain stems and cerebella were removed, and meninges were detached by rolling brains on sterile Whatman paper and then transferred into ice-cold DMEM. Brain tissues were minced by trituration using 25-mL and 10-mL serological pipettes followed by digestion in DMEM medium containing 1 mg/mL collagenase/dispase and 100 µg/mL DNAse I for 45 minutes at 37 °C under shaking. The digestion was stopped by centrifugation at 200g for 10 minutes, and the tissue pellet was resuspended in DMEM containing 20% (w/v) BSA followed by a second centrifugation at 200g for 20 minutes at 21 °C to separate the myelin layer. The upper myelin layer and the supernatant were discarded, and the remaining pellet was washed twice with DMEM endothelial culture medium containing 20% (v/v) fetal calf serum, 10 ng/ mL fibroblast growth factor, 100 ng/mL heparin, 10 000 U/mL penicillin, and 10 mg/mL streptomycin. Cells were cultured for 3 days at 37 °C and 5% CO<sub>2</sub> in dishes precoated with collagen type IV in the presence of 4 µg/mL puromycin to eliminate contaminating cells. Thereafter, puromycin was excluded from culture medium, and BMECs were cultured until confluent. Each biological replicate was prepared from 4 mice per genotype.

#### **Cell Culture and Transfection**

The immortalized mouse brain endothelial cells (bEnd.3) were cultured at 37 °C and 5%  ${\rm CO_9}$  in DMEM medium supplemented with 10% fetal calf serum, 1% minimal essential medium non-essential amino acid solution, 1% glutamax, and 5 µmol/L 2-mercapthoethanol. bEnd.3 and primary BMECs were transfected with pCAGGS-Cavβ3-IRES-GFP, pCAGGS-IP3R1-IRES-GFP, pCAGGS-IP3R3-IRES-GFP, or pCAGGS-IRES-GFP cDNA-encoding plasmids30,31 in the presence of Lipofectamine 3000 following the manufacturer's protocol. pCAGGS indicates plasmid vector for highly efficient expression of genes under the control of the AG promoter and the human CMV-IE enhancer; IRES, internal ribosomal entry site.

#### RNA Isolation and Sequencing

RNA was isolated from wild-type and Cavβ3<sup>-/-</sup> primary BMECs using the RNeasy Mini PLUS Kit following the manufacturer's protocol. The RNA (1 µg total RNA with quality indicator values >8.5) was used for sequencing. RNA solutions (100 µL per sample, at a concentration of 25 ng/ $\mu$ L) were kept at -80 °C until shipped on dry ice to Novogene Europe (Cambridge, United Kingdom) for transcriptome sequencing as described previously.<sup>29</sup>

#### **Western Blot**

BMECs or bEnd.3 cells were harvested by trypsinization followed by lysis in ice-cold lysis buffer containing 50 mmol/L

Tris, 150 mmol/L NaCl, 0.5% sodium deoxycholate, 2 mmol/L EDTA, 50 mmol/L sodium fluoride, 0.1% sodium dodecylsulfate, 1% Nonidet P-40, and 1% Triton X-100 supplemented with complete protease inhibitor cocktail and PhosSTOP. Samples were then incubated at 4 °C for 30 minutes under rotation, followed by centrifugation at 16 900g and 4 °C for 15 minutes. Total protein concentration in the supernatant was determined using a BCA assay, and proteins were denatured in sodium dodecyl sulfate (SDS)-denaturing buffer containing 4% SDS, 60 mmol/L Tris, 0.005% bromophenol blue, 10% glycerol, 5% (v/v) 2-mercapthoethanol, and pH 6.8 for 20 minutes at 60 °C. Denatured proteins were separated by SDS-PAGE (4%-12% NuPAGE Novex Bis-Tris gels) and transferred onto nitrocellulose membrane. After blocking free-binding sites in the presence of nonfat milk, the membranes were incubated with the indicated primary antibodies overnight at 4 °C. Next day, the membranes were incubated with secondary antibodies conjugated to HRP (horseradish peroxidase) or VeriBlot for immunoprecipitation reagent, and bound antibodies were visualized by Western Lightning Chemiluminescence Reagent Plus using the LAS-3000 analyzer (Fujifilm). Membranes used to detect target proteins were stripped and reprobed with loading control antibodies. The following antibodies were used in this study: anti-Cavβ2, anti-Cavβ3, anti-ZO-1, anti-β-actin, anti-CD31/PECAM1, anti-IP3R1, anti-IP3R3, anti-phospho-MLC2, anti-occludin, anti-JAM-A (junctional adhesion molecule-A), and anti-VE-cadherin.

#### **Immunoprecipitation**

For coimmunoprecipitation experiments, wild-type BMECs and bEnd.3 cells (transfected with Cavβ3+IP3R1 or Cavβ3+IP3R3 cDNAs) were lysed in ice-cold lysis buffer (containing 50 mmol/L HEPES, 150 mmol/L NaCl, 1 mmol/L CaCl, 1% [w/v] digitonin, 0.3 µmol/L aprotinin, 10 µmol/L leupeptin, 1 µmol/L pepstatin, 1 µmol/L phenylmethanesulfonyl fluoride, 90 mmol/L iodoacetamid, and 1 µmol/L benzamidine) and incubated for 1 hour at 4 °C, followed by centrifugation at 100 000g for 45 minutes at 4 °C. The supernatant containing protein lysates was incubated in the presence of the anti-Cavβ3 or anti-IP3R1 or anti-IP3R3 antibody coupled to magnetic beads for 2 hours at 4 °C. For high-resolution mass spectrometry, microsomal membrane protein fractions (8 mg) prepared from wild-type or Cavβ3<sup>-/-</sup> mouse brains were homogenized in ice-cold RIPA (radioimmunoprecipitation) buffer and incubated at 4 °C for 30 minutes under rotation, followed by centrifugation at 16 900g and 4 °C for 15 minutes. Supernatants containing the solubilized microsomal membrane proteins were incubated with anti-Cavβ3 or nonspecific rabbit immunoglobulins coupled to magnetic beads for 3 hours at 4 °C. Magnetic beads were collected, extensively washed with the respective lysis buffer, and the bound proteins were eluted and denatured for 20 minutes at 60 °C in the presence of SDS denaturing sample buffer. Denatured proteins were separated by SDS-PAGE (4%-12% NuPAGE Novex Bis-Tris gels) followed by Western blot or high-resolution mass spectrometry.

#### Label-Free High-Resolution Mass Spectrometry

Following antibody-based CavB3 protein enrichment, proteins were eluted, separated on NuPAGE 4% to 12% gradient gels, fixed in the presence of 40% ethanol and 10% acetic acid, and visualized with colloidal Coomassie stain as described

previously.41,42 Four gel pieces were cut, washed, reduced, carbamidomethylated, and trypsin digested. After extraction, tryptic peptides were analyzed by data-dependent nano-LC-ESI-HR-MS/MS (nano-liquid chromatography-electrospray ionization-high resolution-tandem mass spectrometry) analysis. The setup contained Ultimate 3000 RSLCnano LC equipped with Ultimate3000 RS autosampler coupled to a Thermo Scientific Orbitrap Eclipse Tribrid mass spectrometer (Thermo Scientific, Germany). Peptides were separated with a 60- and 120-minute gradient. The 120-minute gradient was generated with buffer A (0.1% formic acid) and buffer B (90% acetonitrile and 0.1% formic acid) at a flow rate of 300 nL/min: 0 to 5 minutes to 4% B, 5 to 80 minutes to 31% B, 80 to 95 minutes to 50% B, 95 to 100 minutes to 90% B, 100 to 105 minutes to 90% B, 105 to 106 minutes to 4% B, and 106 to 120 minutes to 4% B. Tryptic peptides were trapped on a C18 trap column (75 µm×2 cm, Acclaim PepMap100 C18, 3 µm) and separated on a reverse phase column (nano viper Acclaim PepMap C18 capillary column; 2 μm; 75 μm×50 cm). The effluent was sprayed into the mass spectrometer using an emitter (ionization energy, 2.4 keV). MS1 (mass spectrometry 1) peptide spectra were acquired using the Orbitrap analyzer (R, 120 k; radio frequency [RF] lens setting, 30%; m/z=375-1500, MaxIT [maximum injection time]: auto, profile data, intensity threshold of 104). Dynamic exclusion of the 10 most abundant peptides was performed for 60 s. MS2 spectra were collected in the linear ion trap (isolation mode, quadrupole; isolation window, 1.2; activation, higher energy collision induced dissociation [HCD], 30%; scan rate, fast; data type, centroid). Peptides and fragments were analyzed using the TF Proteome Discoverer 1.4 software (Thermo Fisher, Waltham) using the Mascot algorithm (Matrix Science). Briefly, peptides were matched to tandem mass spectra by Mascot, version 2.4.0, by searching of a SwissProt database (version2021\_05; number of protein sequences for all taxonomies, 564638; number of protein sequences for the *Mus musculus* taxonomy, 17 080).

Peptides were analyzed with the following mass tolerances: peptide tolerance, 10 ppm; fragment tolerance, 0.7 D. The Proteome Discoverer workflow included tryptic digest, and we allowed for up to 2 missed cleavage sites. Cysteine carbamidomethylation was set as a fixed modification and deamidation of asparagine and glutamine, acetylation of lysine, and oxidation of methionine were set as variable modifications. The Proteome Discoverer result files were loaded into the Scaffold software (5.3.0; Proteome Software, Inc, Portland, OR) and were combined with Multidimensional Protein-Identification Technology. Peptide identifications were accepted if the parent ion false discovery rate was <5% and contained at least 2 unique identified peptides.

#### Electrophysiology

Wild-type and Cav $\beta$ 3-/- primary BMECs were plated onto collagen-coated glass coverslips and used for patch clamp recordings 24 hours after plating. Whole-cell patch clamp recordings were performed using the Axiovert 135M microscope (Zeiss, Oberkochen, Germany) equipped with the 40× LD Achroplan objective (Zeiss), the EPC9 amplifier (HEKA, Reutlingen, Germany) and the Patchmaster software (HEKA). Patch pipettes were pulled from borosilicate glass capillaries GB150T-8P (Science Products GmbH, Hofheim, Germany) using a vertical puller (PC10; Narishige, Tokyo, Japan) and had resistances between 2 and 4 M $\Omega$  when filled with pipette

solution. Sigmacote (Sigma-Aldrich) was used to coat pipette tips. The bath solution contains (mmol/L) 102 NaCl, 10 CaCl<sub>2</sub>, 5.4 CsCl, 1 MgCl<sub>2</sub>, 20 TEA-Cl, 5 HEPES, and 10 glucose (pH 7.4 with NaOH). Patch pipettes were filled with (mmol/L) 135 CsCl, 3 MgCl<sub>2</sub>, 3 Mg-ATP, 10 EGTA, and 5 HEPES (pH to 7.4 with CsOH). After break-in, voltage ramps spanning from -100 to +100 mV within 50 ms were applied with a repetition every 2 s from a holding potential (Vh) of -60 mV. All ramp currents were corrected for linear leak by auto-leak subtraction using the Patchmaster software (HEKA) and normalized to the cell size (pA/pF).

#### Calcium Imaging

Wild-type, Cavβ3<sup>-/-</sup> BMECs or transfected Cavβ3<sup>-/-</sup> BMECs plated on collagen-coated glass coverslips were loaded with 5 µmol/L Fura-2-AM for 45 minutes at 37 °C protected from light. After washing with the experimental solution containing (in mM) 140 NaCl, 4 KCl, 1 MgCl<sub>9</sub>, 10 HEPES, and 10 glucose (pH adjusted to 7.2 with NaOH), glass coverslips were placed onto the stage of an inverted fluorescence microscope (Axiovert S100; Zeiss, Oberkochen, Germany) equipped with a Fluor-20×/0.75 objective (Zeiss), a Charge-Coupled Device camera (Andor Technology), and a monochromator (polychrome V; TILL Photonics, Gräfelfing, Germany). The described equipment and the analysis of data were controlled by the TILLvisION software (TILL Photonics). Briefly, Fura-2 was alternatively excited at 340 and 380 nm (every 2 s), and the emitted fluorescence was recorded at >440 nm. After background correction, ratio images were calculated from images recorded at 340 and 380 nm (F340/F380). Single endothelial cells were marked as regions of interest and changes in cytoplasmic calcium concentration (Ca2+) are shown as F340/ F380 plotted versus time.

#### **Transendothelial Resistance**

The barrier function of BMEC monolayers (wild type, Cavβ3<sup>-/-</sup>, or transfected Cavβ3<sup>-/-</sup>) or transfected bEnd.3 cell monolayers was measured by the electrical cell-substrate impedance method<sup>43</sup> using the Electric Cell-Substrate Impedance Sensing instrument (Applied BioPhysics, NY). The 96W10idf plate was incubated with a solution containing 10 mmol/L sterile cysteine for 30 minutes to generate stable electrode impedance, followed by washing 3× with sterile water and collagen coating (0.4 mg/mL) for 60 minutes at 37 °C. Next, 2×10<sup>4</sup> BMECs were seeded into the Electric Cell-Substrate Impedance Sensing culture wells (electrodes) and incubated at 37 °C and 5% CO<sub>o</sub>. The resistance was monitored over time at a frequency of 4000 Hz using Electric Cell-Substrate Impedance Sensing Z-Theta (Applied BioPhysics). When resistance values reach a baseline (7-8 days after seeding), thrombin (10 U/ mL), ML-7 (10 μmol/L), YM-254890 (100 nmol/L), Y-27632 (10 µmol/L), U-73122 (10 µmol/L), or vehicle (dimethyl sulfoxide) was applied.

#### In Vitro Permeability Assay

BMECs ( $2.5\times10^6$  cells) were seeded onto collagen-coated transwell culture plate inserts (polyethylene terephthalate membrane,  $0.4~\mu m$  pore size) until they achieved confluency. For permeability measurements, cell culture medium in the lower chamber was replaced by 0.2% BSA in PBS ( $600~\mu L$ ) and in

the upper chamber by 0.2% BSA in PBS (50 µL) supplemented with 1 mg/mL tetramethylrhodamine isothiocyanate—dextran (75 kDa) and 0.25 mg/mL fluorescein isothiocyanate—albumin (66 kDa) in the absence or presence of 10 U/mL thrombin or vehicle. Inserts were then incubated at 37 °C and 5% CO $_2$  for 3 hours. To quantify the passage of fluorescein isothiocyanate—albumin and tetramethylrhodamine isothiocyanate—dextran through the cell monolayer, 20 µL were taken from the upper and lower chambers, transferred into a 96-well plate, and read in the fluorescence plate reader (Tecan Infinite M200). The permeability coefficient (P) was calculated as described at according to the following equation:  $P = \frac{RFU^{lower}}{RFU^{lower}} \times V \times \frac{1}{t} \times \frac{1}{A}$  with RFU being the relative fluorescent unit; V, the volume of the lower chamber in µL; t, the diffusion time in minutes; and A, the total surface area of the monolayer in cm².

#### In Vivo Blood-Brain Barrier Integrity

Blood-brain barrier integrity was determined by Evans blue extravasation according to the study by Fairless et al.45 Adult wild-type and  $Cav\beta3^{-/-}$  mice were anaesthetized with isoflurane, and 2% Evans blue dye was injected into the lateral tail vein at a final dose of 4 mL/kg body weight. After 3 hours, mice were euthanized with an overdose of ketamin/xylazin and transcardially perfused with 20 mL ice-cold PBS to remove intravascular dye. Brain and spinal cord were collected, and the wet weights were determined. To quantify Evans blue contents, the brain and spinal cord were cut into small pieces and incubated in N,N-dimethylformamide for 24 hours at 21 °C. Next, samples were centrifuged at 4000g and the optical density in the supernatant was measured at 595 nm using a plate reader (Tecan Infinite M200). The amount of Evans blue was determined from a standard curve and was normalized to the total tissue weight of each sample.

#### Induction and Evaluation of EAE

 $\text{Cav}\beta3^{-/-}$  and control female mice were immunized as described previously.38 In brief, mice were immunized by subcutaneous injection of 100 µg recombinant MOG<sub>35-55</sub> (myelin oligodendrocyte glycoprotein) peptide in complete Freund's adjuvant containing 10 mg/mL Mycobacterium tuberculosis H37RA (Difco; Fisher Scientific). Immediately after immunization and 48 hours later, mice received intraperitoneal injections of 250 ng of Pertussis toxin (Axxora, Enzo). Over 90% of mice developed disease with no difference between both genotypes. Neurological deficits were scored daily by a blinded experimenter using a scale from 0 to 5 (0, no clinical disease; 0.5, distal paresis of the tail; 1.0, complete paralysis of the tail; 1.5, paresis of tail and mildly impaired righting reflex; 2.0, gait ataxia and severely reduced righting reflex; 2.5, bilateral severe hind limb paresis; 3.0, complete bilateral hind limb paralysis; 3.5, complete bilateral hind limb paralysis and fore limb paresis; 4, hind limb and fore limb paralysis; 5, moribund state or death).

#### Viability/Proliferation Assay

The viability/proliferation assay was performed using CellTiter 96 AQueous One Solution Cell Proliferation Assay Kit according to the manufacturer's protocol and was monitored for 10 days. Briefly, BMECs were seeded onto collagen-coated 96-well plates at a density of  $5\times10^3$  cells per well in 100  $\mu$ L culture medium. Each day, 20  $\mu$ L of CellTiter 96 AQueous One

Solution Reagent was added to each well of a 96-well plate and incubated at 37 °C in 5%  $\rm CO_2$  for 3 hours. The optical density of the colored formazan product at 490 nm was determined by a plate reader (Tecan Infinite M200). It was directly proportional to the number of viable endothelial cells in each well.<sup>46</sup>

#### **IP3 Production Assay**

The IP3 production assay was performed as described previously. In brief, BMECs were seeded onto a collagen-coated white opaque 384-well microplate at a density of  $2\times10^4$  cells per well and cultured until they achieved confluency. Thereafter, medium was changed, and cells were stimulated with 10 or 60 U/mL thrombin in the presence or absence of YM-254890 (100 nmol/L) or U-73122 (10 µmol/L) for 30 minutes at 37 °C in 5% CO $_2$ . The IP3 production before and after agonist stimulation was measured by detecting the inositol monophosphate. The inositol monophosphate is a stable metabolite of IP3 and was measured using the IP-One AlphaLISA Detection Kit following the manufacturer's protocol. The final inositol monophosphate concentration in nanomoles per liter was interpolated from the standard curve using nonlinear regression.

#### **Data Analysis**

Data obtained by Ca2+ imaging and electrophysiological recordings were analyzed using Igor Pro 6.02 (Wavemetrics, OR). GraphPad Prism (version 9.4.1; GraphPad Software, La Jolla, CA) was used to prepare graph presentations, for statistical analysis, and to calculate the P values. Data normality was tested using D'Agostino-Pearson omnibus or Shapiro-Wilk normality tests. Normally distributed data are shown as bar graphs with single values and mean±SD. For non-normally distributed data sets, box and whiskers were used (Tukey box and whiskers, with the boxes extending from the 25th to the 75th percentiles). Whiskers are extended to the most extreme data point that is no more than 1.5× the interguartile range from the edge of the box, and outliers beyond the whiskers are depicted as dots. Statistical analysis and calculation of the P values were performed by unpaired 2-tailed Student t test (normally distributed) or Mann-Whitney U test (non-normally distributed) for comparing 2 experimental groups and 1-way ANOVA (normally distributed) or Kruskal-Wallis test (non-normally distributed) for comparing ≥3 experimental groups. P<0.05 was considered statistically significant.

#### RESULTS

# Cavβ3 Transcripts and Proteins Are Present in Primary BMECs and Have Functions Unrelated to Cav Channel Activity

To visualize *Cacnb3*-expressing cells, we generated a *Cacnb3*-specific *Cre recombinase* knock-in mouse strain (*Cacnb3*-IRES-Cre, *Cacnb3*-IC; Figure S1A through S1E). The *Cacnb3*-IC mice were then crossed with eROSA26- $\tau$ GFP reporter mice<sup>48</sup> to genetically label *Cacnb3*-positive cells by constitutive  $\tau$  *GFP* expression (Figure S1F). GFP-positive cells were identified in brain cryosections from *Cre*-positive mice but not *Cre*-negative mice (Figure 1A). Endothelial cells identified by a positive anti-CD31 (PECAM1) staining were also GFP positive,

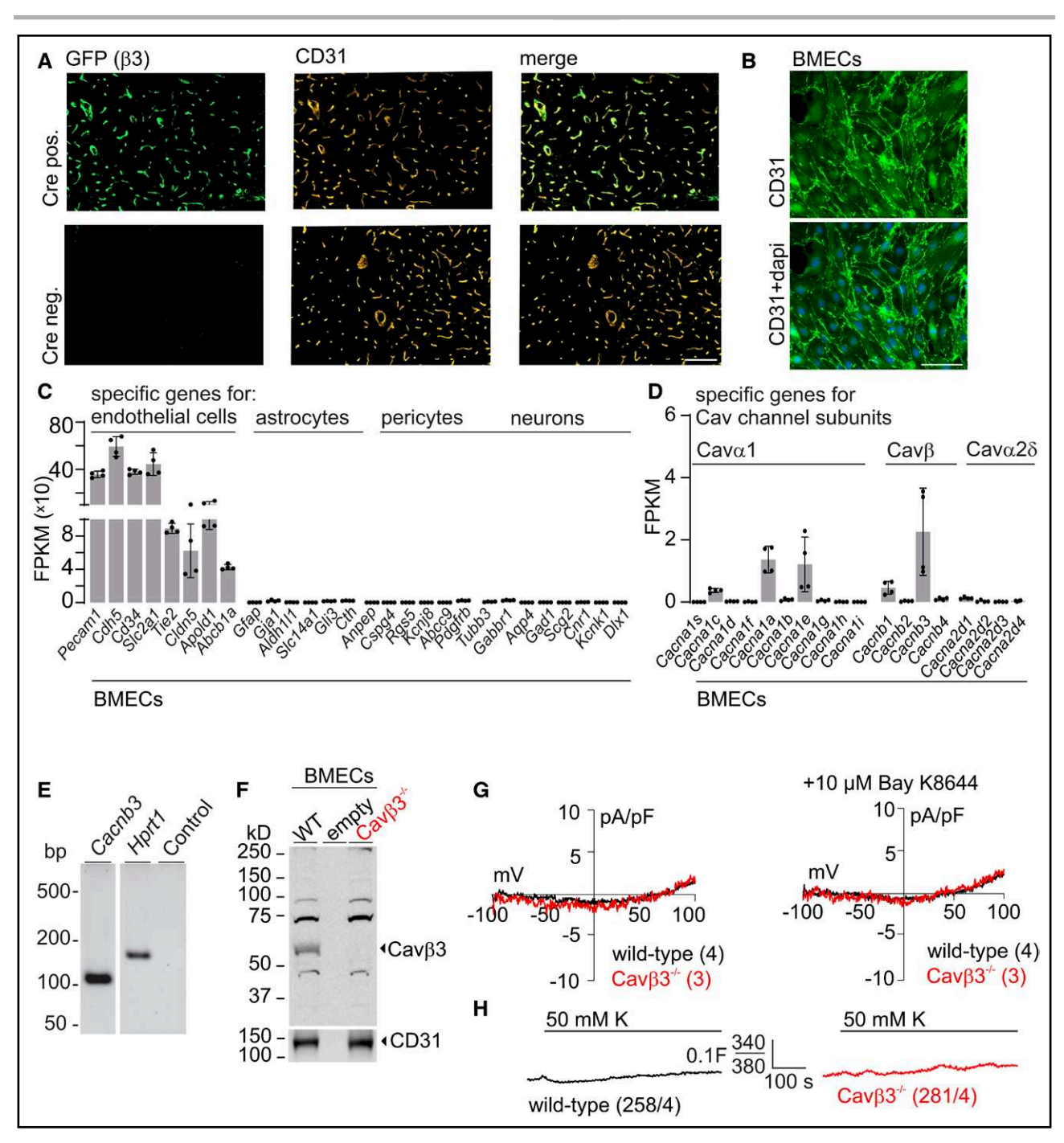


Figure 1. Cavβ3 in primary brain microvascular endothelial cells (BMECs).

A, Representative immunofluorescent images of *Cacnb3*-IRES-Cre-negative (Cre neg.) and Cre-positive (Cre pos.) cortical brain cryosections stained with the endothelial marker anti-CD31 (cluster of differentiation 31; orange) and anti-GFP (green fluorescent protein; green; scale bar=100 μm). The *Cacnb3*-GFP-positive cells were also positive for the endothelial marker CD31 (orange). **B**, Isolated and cultured primary wild-type mouse BMECs stained with anti-CD31 and DAPI (4′,6-diamidino-2-phenylindole). Scale bar=100 μm. **C**, Transcript expression levels of endothelial-, astrocyte-, pericyte-, and neuron-specific genes in isolated BMECs. **D**, Transcript expression levels of the genes of subunits of high voltage-gated Ca²+ channels in BMECs. Data in **C** and **D** are shown as single values of fragments per kilobase of transcript per million mapped reads (FPKM) and bar graphs with mean±SD (n=4 independent BMEC preparations and cultures). **E**, RT-PCR (reverse transcription polymerase chain reaction) of *Cacnb3* and *Hprt1* transcripts with total RNA isolated from BMECs indicating the expression of *Cacnb3* (123 base pairs). *Hprt1* (161 base pairs) was amplified as a positive control, and replacement of RNA by water was used as a negative control. **F**, Western blot of protein extracts from WT (wild-type; black) and Cavβ3<sup>-/-</sup> (voltage-gated Ca²+ channel β3-deficient; red) BMECs using anti-Cavβ3 and anti-CD31 as loading control. **G**, Mean current-voltage relationships recorded from wild-type (black) and Cavβ3<sup>-/-</sup> (red) BMECs by voltage ramps from −100 to +100 mV within 50 ms, which were repeated every 2 s from a holding potential of −60 mV before (**left**) and after (**right**) addition of the L-type Ca²+-channel agonist Bay K8644 (10 μmol/L). The number of measured cells per genotype is indicated in brackets. **H**, Changes in cytoplasmic Ca²+ concentrations, shown as mean Fura-2 (F340/F380) ratiometric traces before and after application of 50 mmol/L potassium in wild-type (black) and Cavβ3<sup>-/-</sup> (red) BMECs. The number

indicating the expression of Cavβ3 transcripts (Figure 1A). We then isolated and cultured primary BMECs from wild-type mice at high purity using a puromycin selection step49 as described by Ruck et al.40 BMECs were identified by the presence of the endothelial protein CD31 (Figure 1B) and by RNA profiling (Figure 1C) of 4 independent isolations and cultures. Endothelial marker genes are expressed in BMEC cultures, whereas expression of marker genes for astrocytes, pericytes, and neurons<sup>50-54</sup> was barely detectable (Figure 1C).

Among the genes expressed in BMECs with a fragments per kilobase of transcript per million mapped reads value >1 (Table S2) were the Cav channel subunit genes Cacna1a, Cacna1e, and Cacnb3, encoding the channel subunits Cav2.1, Cav2.3, and Cavβ3, respectively (Figure 1D). The presence of Cavβ3 transcripts and protein in BMECs was confirmed by RT-PCR (reverse transcription polymerase chain reaction; Figure 1E) and Western blot, using BMECs isolated from  $Cav\beta3^{-/-}$  mice as controls (Figure 1F). Electrophysiological recordings from wild-type and Cavβ3<sup>-/-</sup> BMECs revealed a small (<1 pA/ pF) Cav current that was independent of the presence of Cavβ3 protein and the absence or presence of the Cav channel agonist Bay K8644 (10 µmol/L; Figure 1G). Depolarization of BMECs by potassium (50 mmol/L) in the presence of extracellular Ca2+ did not significantly increase the cytoplasmic Ca<sup>2+</sup> concentration ([Ca<sup>2+</sup>]<sub>a</sub>; Figure 1H). These experiments demonstrate that in BMECs the  $Cav\beta3$  protein is present and may have functions unrelated to its function as a Cav channel subunit.

#### Cavβ3 Contributes to the Maintenance of the Blood-Brain Barrier In Vivo, to the Sealing of **BMEC Monolayers In Vitro and Ameliorates EAE**

Together with other cell types such as astrocytes and pericytes, BMECs form the blood-brain barrier and regulate the exchange of fluids, molecules, and cells between the blood and the central nervous system. To investigate whether Cavβ3 plays a role in maintaining the integrity of the blood-brain barrier in vivo, we generated  $Cav\beta3^{-/-}$  mice (Figure S2) and used them as a control to assess vascular leakage following intravenous injection of Evans blue. Three hours after intravenous injection of Evans blue, mice were euthanized and the extravasation of Evans blue into the brain and spinal cord was determined in wild-type mice and Cavβ3<sup>-/-</sup> mice as controls (Figure 2B). The absence of Cavβ3 protein was confirmed by Western blotting of whole brain protein lysates with an anti-Cavβ3 antibody, which detected Cavβ3 protein (≈55 kDa) in lysates from wild-type mice but not from  $Cav\beta 3^{-/-}$  mice (Figure 2A). The wet weights of brain or spinal cord from wild-type and Cavβ3<sup>-/-</sup> mice were not different (Figure 2C). However, the amount of Evans blue that leaked into the brain and spinal cord was significantly increased in Cavβ3-/- mice compared with

wild-type (Figure 2D), suggesting that the Cavβ3 protein contributes to the integrity of the blood-brain barrier.

BMECs in culture form a continuous monolayer sealed by tight and adherens junctions. To assess the contribution of Cav\u00ed3 protein to the barrier function of these monolayers, transendothelial resistance was measured using the electrical cell-substrate impedance method.<sup>43</sup> After seeding with equal numbers of wild-type and Cavβ3<sup>-/-</sup> BMECs, the cells developed continuous cell monolayers with resistance values reaching the plateau phase at day 5 after seeding (Figure 2E). Both genotypes reached the plateau phase at the same time, but the achieved resistance was significantly reduced on days 4, 5, 6, and 7 in  $Cav\beta 3^{-/-}$  BMECs compared with cells from wild-type animals (day 7: wild-type, 3113 $\pm$ 122.1 $\Omega$  [n=45]; Cav $\beta$ 3<sup>-/-</sup>, 2441 $\pm$ 92.7 $\Omega$  [n=34]; P<0.0001). The absence of Cavβ3 had no effect on endothelial cell viability and proliferation over 10 days (Figure 2F). Independently, the contribution of Cavβ3 protein to the barrier function of BMEC monolayers was assessed by their permeability to albumin or dextran. The leakage rate for albumin and dextran was significantly higher in  $Cav\beta3^{-/-}$  monolayers than in BMEC monolayers from wild-type animals (Figure 2G).

To examine the influence of Cavβ3 on the blood-brain barrier during neuroinflammation of the central nervous system, we immunized wild-type and  $\text{Cav}\beta3^{-\!/\!-}$  mice with  $MOG_{35-55}$  for EAE induction (Figure 2H) and followed the clinical disability in mice over 30 days.  $Cav\beta 3^{-/-}$  mice showed a more severe EAE disease course (Figure 2I) with increased cumulative clinical disability (Figure 2J) and earlier disease onset (Figure 2K) compared with wildtype control mice. Furthermore, on day 5 following EAE symptom onset, the amount of Evans blue that leaked into the brain was significantly increased in Cavβ3-/mice compared with wild-type mice (Figure 2L). In agreement with the increased clinical disability and increased permeability of the blood-brain barrier, the number of CD3-positive T cells infiltrating the spinal cord was significantly increased at the acute phase (5 days following symptom onset) and slightly (P=0.0908) increased at the chronic phase (21 days following symptom onset) of EAE in  $Cav\beta3^{-/-}$  compared with wild-type mice (Figure 2M). Demyelination measured by Luxol fast blue staining was slightly, but not significantly, increased in Cavβ3<sup>-/-</sup> at the acute phase of EAE (Figure 2N). In summary, Cavβ3 protein appears to help maintain the integrity of the bloodbrain barrier, reduces immune cell infiltration, and thereby alleviates the clinical symptoms of EAE in mice.

#### Increased Thrombin-Induced Endothelial Barrier Disruption in the Absence of Cavβ3

Thrombin is a proinflammatory mediator and increases endothelial permeability. Therefore, we determined the thrombin-induced changes in transendothelial electrical

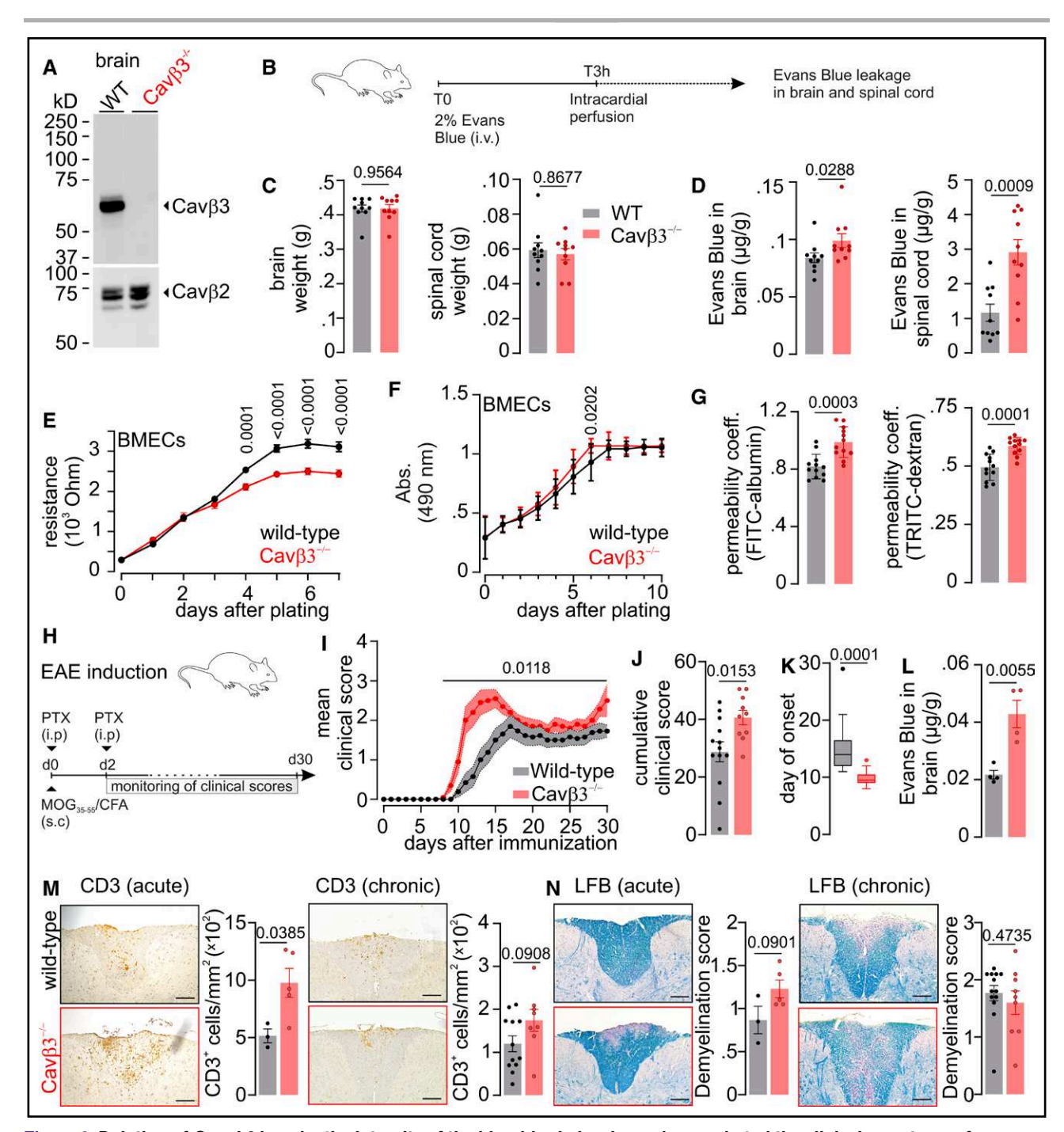


Figure 2. Deletion of *Cacnb3* impairs the integrity of the blood-brain barrier and exacerbated the clinical symptoms of experimental autoimmune encephalomyelitis.

A, Western blot of protein extracts from WT (wild-type; black) and Cavβ3<sup>-/-</sup> (voltage-gated Ca²+ channel β3-deficient; red) brains (100 μg of protein per lane) using anti-Cavβ3 and as a loading control anti-Cavβ2 antibody. **B**, Protocol followed for the assessment of the integrity of the blood-brain barrier in vivo with time points for Evans blue administration and analysis indicated. **C**, Brain (**left**) and spinal cord (**right**) wet weights measured after Evans blue injection and transcardial perfusion with PBS (n=10 mice). **D**, Amount of Evans blue extravasation into the brain (**left**) and spinal cord (**right**) of wild-type (black) and Cavβ3<sup>-/-</sup> (red) mice shown as μg Evans blue per g tissue weight (μg/g; n=10 mice). **E**, Mean transendothelial resistance of wild-type (black) and Cavβ3<sup>-/-</sup> (red) brain microvascular endothelial cell (BMEC) monolayers, monitored for 7 days from the initial seeding of 20 000 cells per well (n=45 wells for wild-type [black] and 34 wells for Cavβ3<sup>-/-</sup> [red] BMECs from 3 independent BMEC preparations and cultures). **F**, Metabolic activity and proliferation of wild-type (black) and Cavβ3<sup>-/-</sup> (red) BMECs monitored by conversion of the added tetrazolium into colored formazan, determined as optical density at 490 nm (Abs. n=12 wells from 4 independent BMEC preparations and cultures). **G**, In vitro permeability of BMEC monolayers (wild-type, black; Cavβ3<sup>-/-</sup>, red) for fluorescein isothiocyanate (FITC)–albumin (66 kDa, **left**) and tetramethylrhodamine isothiocyanate (TRITC)–dextran (75 kDa, **right**) measured as permeability coefficients (coeff., n=12 wells from 4 independent BMEC preparations). **H**, Schematic representation of experimental procedure followed to induce experimental autoimmune encephalomyelitis (EAE). **I**, Disease course following induction of EAE in wild-type (black) and (*Continued*)

resistance of wild-type and Cavβ3<sup>-/-</sup> BMEC monolayers (Figure 3A and 3B). Application of thrombin resulted in a transient decrease in transendothelial resistance of wildtype BMEC monolayers and returning to basic values within 2 hours after thrombin exposure (Figure 3A and 3B). In contrast, exposure of  $Cav\beta 3^{-/-}$  BMEC monolayers to thrombin resulted in a significantly greater decrease, which did not return to baseline within 2 hours of thrombin exposure (Figure 3A and 3B). Moreover, expression of Cacnb3 cDNA in Cavβ3-/- BMEC monolayers (Figure 3C and 3D) rescued the wild-type barrier function phenotype, leading to a significantly smaller effect in thrombin-mediated transient decrease in transendothelial resistance and improved recovery to baseline. Similarly, overexpression of the Cacnb3 cDNA in bEnd.3 cells (Figure S3A and S3B) reduced thrombin-mediated transient decrease in transendothelial resistance compared with mock-transfected cells (Figure S3C and S3D). In both Cavβ3<sup>-/-</sup> and wild-type, the permeability of BMEC monolayers to albumin and dextran was significantly increased in the presence of thrombin (Figure 3E). However, thrombin-induced increase in dextran permeability was significantly more pronounced in  $Cav\beta 3^{-/-}$  monolayers compared with wild-type monolayers (wild-type,  $0.080\pm0.003$ ; Cav $\beta$ 3<sup>-/-</sup>,  $0.097\pm0.005$ ; P=0.0303).

To investigate potential changes in cell morphology and tight and adherens junctions of the endothelium, the organization of the junctional protein ZO-1 in wild-type and  $Cav\beta3^{-/-}$  BMECs in the presence or absence of thrombin was examined by immunofluorescence staining (Figure 3F). The size of endothelial cells (Figure 3G) and the amounts of ZO-1 per µg of endothelial protein (Figure 3H and 3I) were significantly reduced in Cavβ3<sup>-/-</sup> cells, as was the length of continuous ZO-1 staining between adjacent cells (Figure 3J). In contrast, the number of disrupted tight junctions per cell was only slightly higher in the absence of Cavβ3 (Figure 3K).

In the presence of thrombin, ZO-1 staining was less well organized along cell borders and the number of cells with disrupted tight junctions was increased (Figure 3F, 3J, and 3K). At the same time, thrombin-induced disruption of ZO-1 junction protein was more pronounced in the absence of Cavβ3 protein. However, protein levels of vascular endothelial cadherin, JAM-A, and occludin were apparently the same in both genotypes (Figure S5C).

Thus, in the absence of Cavβ3, the length of continuous ZO-1 staining between adjacent cells was decreased and the size of endothelial cells was reduced while the thrombin-mediated permeability of BMEC monolayers was increased.

#### Removal of Cavβ3 Enhances Thrombin-Mediated Ca<sup>2+</sup> Release Without Affecting Intracellular Ca2+ Stores and IP3 Formation

Thrombin increases endothelial permeability through activation of G-protein-coupled PAR-1, followed by IP3 formation and IP3-induced Ca2+ release from intracellular stores (Figure 4A). The resting cytoplasmic Ca<sup>2+</sup> concentration before thrombin application and the thrombin-induced Ca2+ increase (peak amplitude and area under the curve) were significantly enhanced in Cavβ3<sup>-/-</sup> BMECs compared with wild-type control BMECs (Figure 4A and 4B). Moreover, the expression of Cacnb3 cDNA in Cav $\beta3^{-/-}$  BMECs efficiently rescued wild-type Ca2+ signaling, leading to a significant decrease in thrombin-induced Ca2+ release compared with mock-transfected Cavβ3<sup>-/-</sup> BMECs (Figure 4C and 4D). The accumulation of inositol monophosphate, a stable downstream metabolite of IP3, was then measured in response to thrombin stimulation in the absence or presence of the  $G\alpha_{\alpha/11}$ -specific inhibitor YM-254890 or the phospholipase C inhibitor U-73122 (Figure 4E). Thrombin increased IP3 formation in a concentrationdependent manner and this effect was inhibited by YM-254890 or U-73122. The IP3 formation before and after the addition of thrombin was not significantly different in BMECs of both genotypes (Figure 4E).

Thrombin-induced Ca2+ release after receptor stimulation is increased in Cavβ3<sup>-/-</sup> BMECs compared with wild-type BMECs (Figure 4A through 4D), and storeoperated Ca2+ entry may be altered in these cells. Therefore, stores were depleted by thapsigargin in the absence of extracellular Ca2+. Again, in this experiment, resting Ca2+ levels were significantly increased in Cavβ3<sup>-/-</sup> BMECs before thapsigargin application (Figure S4A and S4B). The thapsigargin-induced increase in cytoplasmic Ca2+ in the absence of extracellular Ca2+ was not different in cells of both genotypes (Figure S4A and S4B), indicating that the Ca2+ content of intracellular

Figure 2 Continued. Cavβ3<sup>-/-</sup> (red) mice (wild-type, n=13; Cavβ3<sup>-/-</sup>, n=10). J and K, Cumulative clinical disability score (J) and day of disease onset of clinical symptoms following induction of EAE (**K**; wild-type, n=13; Cavβ3<sup>-/-</sup>, n=10). **L**, Amount of Evans blue extravasation into the brain of wild-type (black) and Cavβ3<sup>-/-</sup> (red) mice measured during the acute stage of EAE (5 days following symptom onset) and shown as μg Evans blue per g tissue weight (µg/g; n=4 mice). M, Representative histopathologic staining and quantifications of CD3 (cluster of differentiation 3)-positive T cells in cervical spinal cord sections during the acute (left) and chronic (right, 21 days following symptom onset) phases of EAE. The number of CD3-positive T cells are normalized to the spinal cord area, and each data point represents an individual mouse. Scale bar=100 µm. N, Representative histopathologic staining of Luxol fast blue (LFB) in cervical spinal cords and quantifications of demyelination (LFBpositive area) during the acute (left) and chronic (right) phases of EAE. Each data point represents an individual mouse. Scale bar=100 µm. Data are shown as mean ±SD (C, D, F, G, J, L, M, and N), mean ±SEM (E and I), or Tukey box and whiskers (K), and P values were determined by unpaired 2-tailed Student t test (C-G, J, L, M, and N), Mann-Whitney U test of the area under the curve (AUC) of each animal (I), or Mann-Whitney U test (K). CFA indicates complete Freund's adjuvant; MOG, myelin oligodendrocyte glycoprotein; and PTX, pertussis toxin.

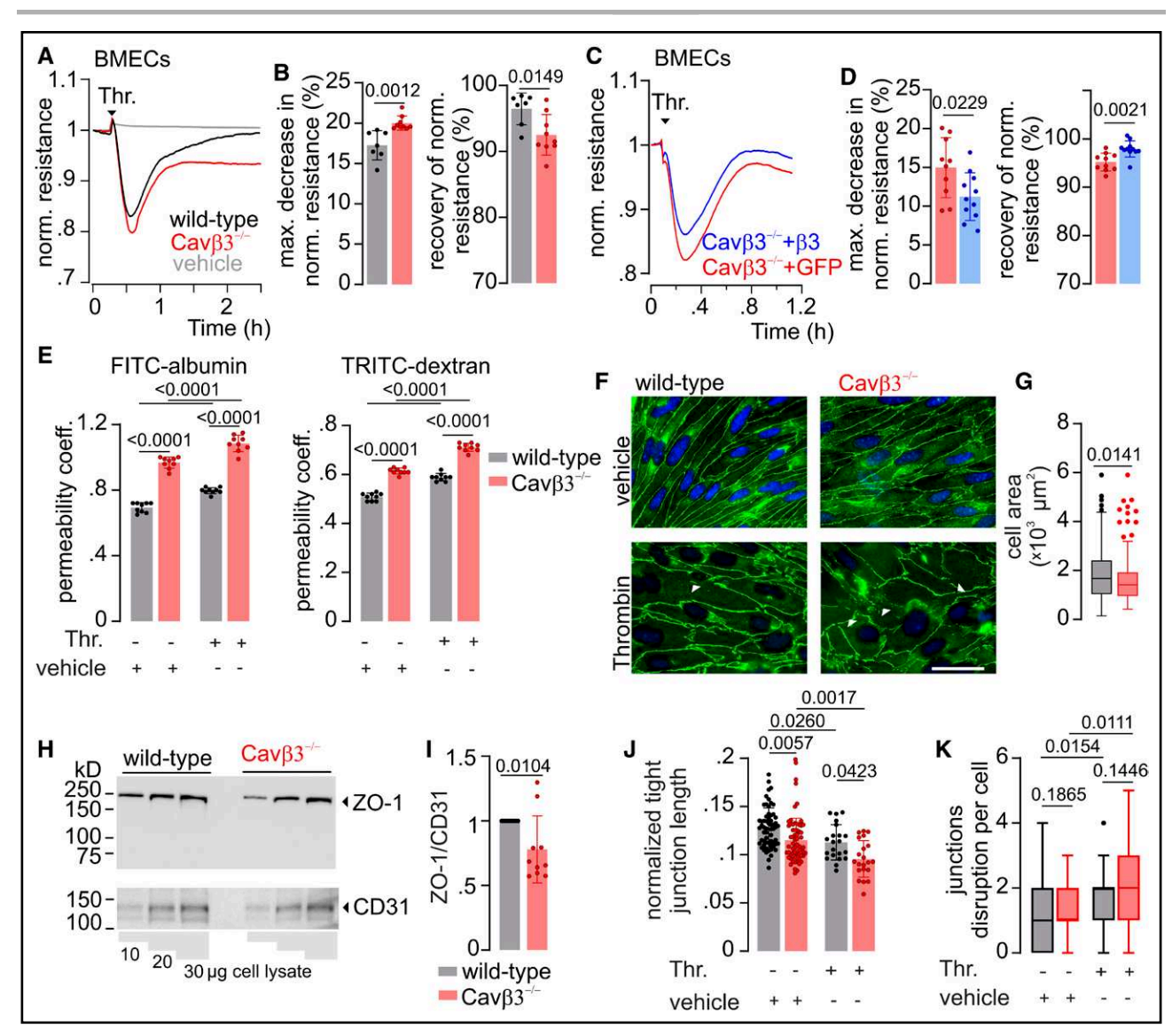


Figure 3. Deletion of Cavβ3 enhances thrombin (Thr.)-induced endothelial barrier disruption.

A and C, Mean normalized (norm.) resistance (from 1 independent experiment, repeated 2x) measured in confluent brain microvascular endothelial cell (BMEC) monolayers from wild-type (black) and  $Cav\beta^{3-/-}$  (voltage-gated  $Ca^{2+}$  channel  $\beta 3$ -deficient; red; **A**) or from  $Cav\beta^{3-/-}$ transfected with Cavβ3 cDNA (blue) or IRES-GFP (green fluorescent protein) cDNA (red; C) and monitored over time in the absence and presence of Thr. (10 U/mL) or vehicle (gray) as indicated. B and D, Percentage (%) of maximal (max.) decrease in norm. resistance (left) and recovery of norm. resistance over time (right) in response to the application of Thr. measured in confluent BMEC monolayers from wild-type (black) and Cavβ3<sup>-/-</sup> (red) mice (**B**, n=7 wells for wild-type and 9 wells for Cavβ3<sup>-/-</sup> from 2 independent preparations and cultures) or from Cavβ3<sup>-/-</sup> transfected with Cavβ3 (blue) or IRES-GFP (red; **D**, n=10 wells for cells transfected with Cavβ3 and 11 for IRES-GFP). E, Permeability coefficient of FITC-albumin (left) and tetramethylrhodamine isothiocyanate (TRITC)-dextran (right) of wild-type (black) and Cavβ3<sup>-/-</sup> (red) BMEC monolayers in the absence (-) or presence (+) of Thr. (10 U/mL) or vehicle (n=9 wells from 5 independent preparations and cultures). F, Representative immunofluorescence images from wild-type and Cayβ3-- BMECs stained with anti-ZO-1 (zona occludens-1) antibody for tight junctional protein ZO-1 (green) and DAPI (4',6-diamidino-2-phenylindole) for nuclei (blue). The images show tight junction morphology in confluent BMECs treated for 3 hours with Thr. (10 U/mL) or vehicle as control. Examples of disrupted tight junctions are labeled by white arrowheads (scale bar=40 µm). G, Cell area (in µm²) measured from ZO-1 immunofluorescence images (as in F) of wild-type (black) and Cavβ3<sup>-/-</sup> (red) BMECs (n=215 cells from 5 independent preparations). **H**, Western blot of protein extracts from wild-type and Cavβ3<sup>-/-</sup> BMECs using anti-ZO-1 antibody and as a loading control, anti-CD31 (cluster of differentiation 31; bottom). I, Intensity of the ZO-1 antibody stain normalized to the CD31 antibody stain obtained from 3 independent Western blots. J. Continuous tight junction length normalized to the cell area measured from ZO-1 immunofluorescence images (as in **F**) of wild-type (black) and Cavβ3<sup>-/-</sup> (red) BMECs in the presence of Thr. (10 U/mL) or vehicle, as indicated (n=21-61 cells from 4 independent preparations). K, Numbers of ZO-1 junctional disruptions per cell counted from ZO-1 immunofluorescence images (as in F) of wild-type (black) and Cavβ3<sup>-/-</sup> (red) BMECs in the presence of Thr. (10 U/mL) or vehicle as indicated (n=50 cells from 4 independent preparations). Data are shown as mean±SD (B, D, E, I, and J) or Tukey box and whiskers (G and K) and P values were determined by unpaired 2-tailed Student t test (B, D, and I), Mann-Whitney U test (G), 1-way ANOVA followed by Tukey multiple comparison test (**E** and **J**) or Kruskal-Wallis test (**K**). IRES indicates internal ribosomal entry site.

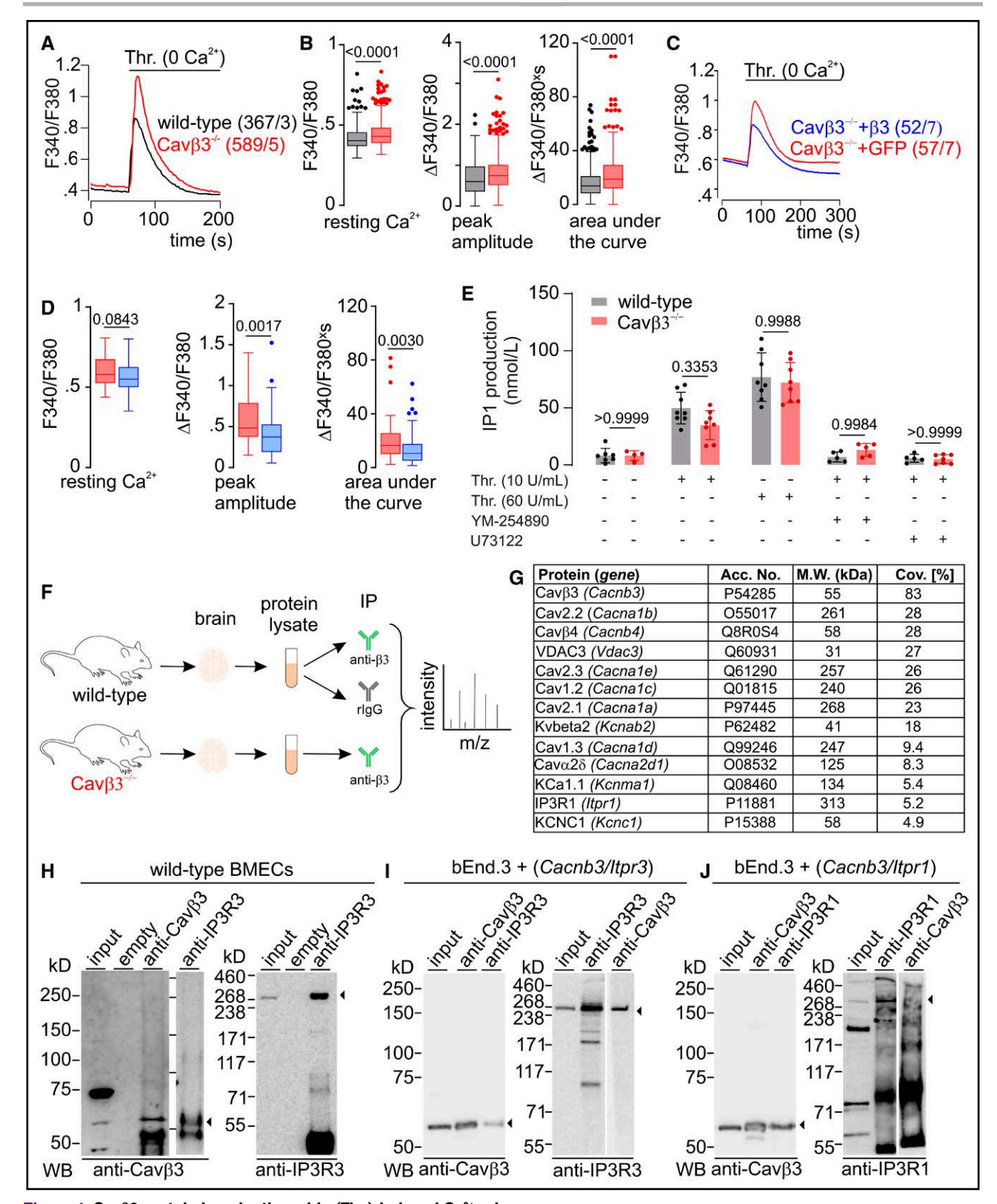


Figure 4. Cavβ3 protein impairs thrombin (Thr.)-induced Ca²+ release.

A and C, Changes in cytoplasmic Ca²+ concentration, shown as mean Fura-2 (F340/F380) ratiometric traces before and after the application of Thr. (10 U/mL) in the absence of extracellular Ca²+ measured in wild-type (black) and Cavβ3<sup>-/-</sup> (voltage-gated Ca²+ channel β3-deficient; red) brain microvascular endothelial cells (BMECs; A) and Cavβ3<sup>-/-</sup> BMECs transfected with Cavβ3 (blue) or IRES-GFP (green fluorescent protein) cDNAs (red; C). The number of measured cells (x) per experiment (y) is indicated as (x/y). B and D, Resting Ca²+ levels before Thr. application (left), peak amplitudes (middle), and area under the curve (right) of the Thr.-induced Ca²+ release from experiments in A and C. E,

Inositol monophosphate (IP1) accumulation (nmol/L) in wild-type (black) and Cavβ3-/- (red) BMECs before and after application (Continued)

stores was not affected in the absence of  $Cav\beta 3$ . After the cytoplasmic  $Ca^{2+}$  level decreased to baseline, extracellular  $Ca^{2+}$  was readded, resulting in  $Ca^{2+}$  entry through plasma membrane channels.  $Ca^{2+}$  entry, calculated as peak amplitude and area under the curve, was not different in BMECs of both genotypes (Figure S4A and S4C).

Previously, we showed<sup>29,31</sup> that Cavβ3 interacts with the inositol 1,4,5-trisphosphate receptors (IP3Rs) and reduces binding of [3H]IP3 to the IP3R and modulates IP3-dependent Ca2+ signals by applying coimmunoprecipitation and in vitro binding experiments. Here, we verified the interaction of Cavβ3 with the IP3Rs by 2 approaches in the whole mouse brain, in primary microvascular endothelial cells (BMECs) isolated from mouse brain, and in bEnd.3 cells. In the first approach, we prepared and solubilized brain microsomal proteins from wild-type and  $Cav\beta3^{-/-}$  mice to enrich the  $Cav\beta3$ protein-containing complex using the anti-Cavβ3 antibody. Bound proteins were eluted, were separated by SDS-PAGE, and Cavβ3 peptides covering 83% of the primary sequence were identified by mass spectrometry (nano-LC-ESI-MS/MS; Figure 4F; Figure S5A). In addition, 147 proteins were specifically associated with Cavβ3 (Figure 4G; Table S1). As negative controls, we used (1) microsomal protein lysate from Cavβ3<sup>-/-</sup> brain and (2) target-unrelated antibodies (Figure 4F, rabbit IgG). Among those 147 proteins, ion channel proteins including IP3R1 were identified (Figure 4G; Figure S5B). In the second approach, we verified Cavβ3-IP3R interaction in wild-type BMECs (where both proteins are present) and in bEnd.3 cells after overexpressing the Cacnb3 cDNA with either Itpr1 or Itpr3 cDNAs. In wild-type mouse BMECs, Cavβ3 was associated with IP3R3 in the coimmunoprecipitation using the anti-IP3R3 antibody (Figure 4H). Moreover, in bEnd.3 cells, Cavβ3 was coimmunoprecipitated with IP3R3 and IP3R1 and vice versa using anti-Cav $\beta$ 3, anti-IP3R3, and anti-IP3R1 antibodies (Figure 4I and 4J). These results support an interaction between Cavβ3 and IP3R in BMECs and demonstrate that Cavβ3 in endothelial cells tightly controls resting cytoplasmic Ca2+ levels and thrombin-mediated Ca2+ release from the intracellular IP3-sensitive Ca2+ stores

without affecting the IP3 generation pathway, intracellular Ca<sup>2+</sup> stores, or store-operated Ca<sup>2+</sup> entry.

## Cavβ3 Contributes to Endothelial Barrier Integrity by Controlling Ca<sup>2+</sup>-Dependent MLC Phosphorylation

Thrombin induces Ca<sup>2+</sup>-dependent activation of MLCK and RhoA/Rho kinase-dependent inhibition of myosin phosphatase.55 Both signaling pathways promote MLC phosphorylation, leading to impaired endothelial barrier function. Thus, in the presence of thrombin, MLC phosphorylation in BMECs increases in a timedependent manner (Figure 5A and 5B), with the amount of phosphorylated MLC significantly increased in Cavβ3<sup>-/-</sup> BMECs compared with wild-type BMECs at 5 and 15 minutes (Figure 5A and 5B). The MLCK inhibitor ML-7 decreased thrombin-mediated phosphorylation of MLC (Figure 5C), while abolishing the disorganization of ZO-1 (Figure 5D and 5E). In the presence of ML-7 or the  $G\alpha_{\alpha/11}$  inhibitor YM-254890, the decrease in transendothelial resistance in BMECs of both genotypes is significantly less than in the absence of either inhibitor (Figure 5F, 5G, and 5H). The significantly greater decrease in resistance in  $Cav\beta3^{-/-}$  BMECs in the absence of inhibitors (Figure 5F, 5G, and 5H; Figure 3A and 3B) is no longer detectable in the presence of either inhibitor (Figure 5F, 5G, and 5H). Similarly, the decrease in transendothelial resistance is reduced in the presence of U-73122 but is no longer different in both genotypes (Figure 5I, 5J, and 5K). In contrast, the magnitude of the decrease in thrombin-induced transendothelial resistance in  $Cav\beta 3^{-/-}$  BMECs and wild-type BMECs is little changed in the absence and presence of the Rho kinase inhibitor Y-27632. Notably, the significant difference between the 2 genotypes remains (Figure 5I, 5J, and 5K). In conclusion, the results show that Cavβ3 contributes to the control of Ca2+-dependent MLC phosphorylation and thus to the integrity of the endothelial barrier. In contrast, Cavβ3 has only a minor effect on the Rho kinase pathway, which is simultaneously activated by thrombin.

Figure 4 Continued. of Thr. (10 and 60 U/mL) in the presence of YM-254890 (100 nmol/L) or U-73122 (10 μmol/L) as indicated (n=5-8 wells). Thr. application induced a significant (*P*<0.05) increase of IP1 accumulation in both genotypes. Data are shown as Tukey box and whiskers (**B** and **D**) or mean±SD (**E**) and *P* values were determined by Mann-Whitney *U* test (**B** and **D**) or 1-way ANOVA followed by Tukey multiple comparison test (**E**). **F**, Workflow of antibody-based Cavβ3 protein enrichment from mouse brain lysates combined with mass spectrometry. **G**, Identification of the Cavβ3 protein (sequence coverage, 83%) from wild-type mouse brain after antibody-based enrichment followed by mass spectrometry. Table shows ion channel proteins associated with the Cavβ3 protein detected in purifications from 2 independent wild-type brain preparations using specific anti-Cavβ3 antibody and were absent in negative controls: anti-Cavβ3-based enrichment from Cavβ3<sup>-/-</sup> brain lysates and enrichment from wild-type brain lysates using a target-unrelated antibody (rabbit immunoglobulin [rlgG]). **H** through **J**, Coimmunoprecipitations with anti-Cavβ3, anti-IP3R1, and anti-IP3R3 from solubilized wild-type BMECs (**H**), b.End3 transfected with *Cacnb3+ltpr3* cDNAs (**I**), or b.End3 transfected with *Cacnb3+ltpr1* cDNAs (**J**). Input and proteins eluted from the precipitating antibodies were subjected to Western blot (WB) and probed with anti-Cavβ3 (left blots), anti-IP3R3 (right blot in **H** and **I**), or anti-IP3R1 (right blot in **J**). Empty indicates that nothing was applied into the SDS-PAGE; arrowhead, target protein. Acc. No. indicates accession number UniProtKB; Cov. [%], percentage of sequence coverage; IP3R, inositol 1,4,5-trisphosphate (IP3) recetor; IRES, internal ribosomal entry site; M.W., molecular weight; and SDS, sodium dodecyl sulfate.

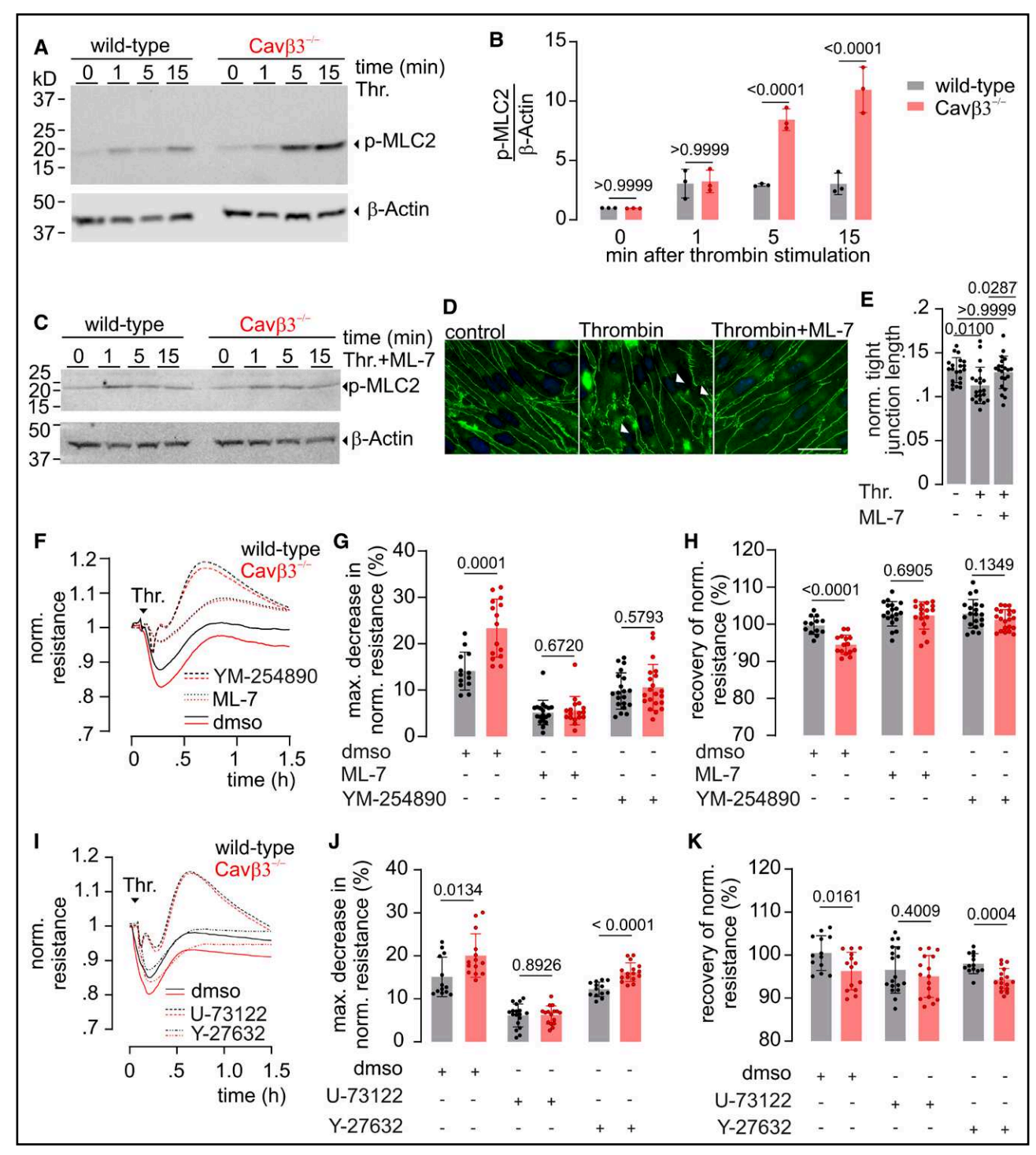


Figure 5. Cavβ3 controls the activity of MLCK (myosin light chain kinase) and the phosphorylation of MLC (myosin light chain). A and C, Western blot of protein extracts (30 μg of protein per lane) from wild-type and Cavβ3<sup>-/-</sup> (voltage-gated Ca²+ channel β3-deficient) brain microvascular endothelial cells (BMECs) using anti-phospho-myosin light chain 2 (p-MLC2) and anti-β-actin as a loading control. Cells were incubated in the absence and in the presence of thrombin (Thr.; 10 U/mL) for 1, 5, and 15 minutes in the absence (A) or presence of ML-7 (C). B, Intensity of the p-MLC2 antibody stain normalized to the β-actin antibody stain obtained from 3 independent Western blots as shown in A. D, Representative immunofluorescence images from wild-type BMECs stained with anti-ZO-1 (zona occludens-1) antibody for tight junctional protein ZO-1 (green) and DAPI (4′,6-diamidino-2-phenylindole) for nuclei (blue). The images show tight junction morphology in confluent BMECs treated for 3 hours with vehicle (control), Thr., or Thr.+ML-7. Examples of disrupted tight junctions are labeled by white arrowheads (scale bar=40 μm). E, Continuous tight junction length normalized to the cell area measured from ZO-1 immunofluorescence images (as in D) of wild-type BMECs in the absence (–) or presence (+) of Thr. (10 U/mL) or of Thr.+ML-7 (10 μmol/L) as indicated (n=21 cells from 4 independent preparations). F and I, Mean normalized (norm.) resistance (representative for 1 independent experiment, repeated 4×) measured in wild-type (black) and Cavβ3<sup>-/-</sup> (red) confluent BMEC monolayers (n=13–20 wells for wild-type and 14–21 wells (*Continued*)

### Transcriptome Profiling of Primary Wild-Type and Cavβ3<sup>-/-</sup> BMECs

To evaluate the role of Cavβ3 in the regulation of gene expression in BMECs, which may be related to the increased permeability of the blood-brain barrier in  $\text{Cav}\beta3^{-/-}$  mice, we prepared 4 independent BMEC cultures from wild-type and  $Cav\beta3^{-/-}$  mice, isolated RNA, and performed bulk RNA sequencing for transcriptome profiling. In  $Cav\beta3^{-/-}$  BMECs, 463 genes were downregulated and 549 genes were upregulated (Figure 6A and 6B; Table S2). The differentially downregulated genes in  $Cav\beta3^{-/-}$  BMECs included genes involved in Ca<sup>2+</sup> signaling (*Itpr1*), solute carrier-mediated transport (Slc5a3, Slc1a1, and Slc44a1), tight and adherens junctions (Ocln, Jam1, Pecam1, and Nectin2), cell surface and cytoskeleton (Alcam and Tns 1), as well as genes of basement membrane proteins and integrins (Lama4) and Itga 1), and matrix metalloproteinases (Adam 15 and Adam 17; Figure 6C; Table S2). Gene ontology (molecular function, biological process, and cellular components) analysis of differentially expressed transcripts revealed that cell adhesion and cell-cell junction were among the enriched terms (Figure 6D; Figure S6A and S6B). Collectively, these results indicate that deletion of the Cav\u03B3 encoding gene Cacnb3 affects pathways associated with endothelial cell function, which may additionally impact the endothelial barrier permeability.

#### **DISCUSSION**

By crossing the *Cacnb3*-specific Cre recombinase knock-in mouse strain (*Cacnb3*-IC; Figure S1) with eROSA26- $\tau$ GFP reporter mice, <sup>48</sup> *Cacnb3*-positive cells were visualized by constitutive  $\tau$ GFP expression (Figure S1F). *Cacnb3*-positive cells in the brain included CD31-positive BMECs (Figure 1A). We isolated CD31-positive BMECs from mouse brain and by RNA sequencing, and RT-PCR detected Cav $\beta$ 3 (*Cacnb3*) transcripts (Figure 1D and 1E). By Western blotting (Figure 1F), the Cav $\beta$ 3 protein was recognized by anti-Cav $\beta$ 3 antibodies in BMECs from wild-type mice but not in the BMECs isolated from Cav $\beta$ 3-/- mice.

Endothelial cells are considered nonexcitable, and it is difficult to relate the slow and often small changes in membrane potential in these cells to the activation of Cav channels. We detected transcripts of *Cacna1a* and *Cacna1e* (Figure 1D) and recorded small, Bay K8644–independent voltage-gated currents (Figure 1G), which

may represent P-type (Cav2.1) and R-type (Cav2.3) Cav currents. The R-type Ca²+ channel was thought to be important for activation of endothelial cells by platelet-activating factor. However, the recorded currents were not dependent on the presence of Cav $\beta$ 3. In addition, potassium depolarization of the cells did not increase the cytoplasmic Ca²+ concentration (Figure 1H), suggesting a function of Cav $\beta$ 3 independent of its role as a Cav channel subunit.

BMECs are part of the blood-brain barrier. By injecting Evans blue into wild-type and Cav $\beta3^{-/-}$  animals, we investigated the integrity of the blood-brain barrier in vivo. In parallel, we determined the permeability to dextran and albumin in monolayers of wild-type and Cav $\beta3^{-/-}$  BMECs in vitro. Both in vivo and in vitro, permeability was increased in the absence of Cav $\beta3$  (Figure 2), suggesting that the Cav $\beta3$  subunit contributes to the integrity of the permeability barriers.

Blood-brain barrier permeability is increased in patients with multiple sclerosis<sup>57</sup> and has a significant impact on the course of EAE in mice. 58,59 Cavβ3<sup>-/-</sup> mice with compromised blood-brain barrier exhibited greater T-cell infiltration during EAE, developed more severe clinical disability, and had significantly earlier onset of disease symptoms than wild-type mice (Figure 2H through 2N). The impaired blood-brain barrier in  $Cav\beta3^{-/-}$  mice may explain the enhanced infiltration of T cells and the increased disease symptoms. In the brain, Cavβ3 preferentially, but not exclusively, associates with the Cav2.2 α1B pore-forming subunit of N-type Cav channels<sup>60-64</sup> and deletion of Cav $\beta$ 3 reduces Cav2.2  $\alpha$ 1B expression in dorsal root ganglion<sup>62</sup> and sympathetic neurons.<sup>63</sup> However, in contrast to our observations in Cavβ3<sup>-/-</sup> mice, deletion of the Cacna1b gene in Cav2.2 knockout mice significantly ameliorated the disease course of EAE,65 suggesting that Cavβ3 plays a role independent of its function as a subunit of Cav channels.

In previous studies, we have shown that  $\text{Cav}\beta3$  reduces IP3-dependent  $\text{Ca}^{2+}$  release from intracellular stores by reducing the sensitivity of the cell to low IP3 concentrations through binding to the IP3 receptor. In the present study, we confirm the interaction of  $\text{Cav}\beta3$  with the IP3R by coimmunoprecipitation in primary BMECs and bEnd.3 cells and by antibody-based enrichments of the  $\text{Cav}\beta3$  protein and associated proteins followed by nano-LC-MS/MS analysis in whole brain lysate (Figure 4F through 4J). Consistent with previous reports, the pore-forming  $\alpha1$  subunits of Cav2.1, Cav2.2, and Cav2.3 were also effectively

Figure 5 Continued. for Cavβ3<sup>-/-</sup> from 2 independent preparations) and monitored over time after application of Thr. (10 U/mL, arrowhead). The monolayers were pretreated for 3 hours with ML-7 (10 μmol/L), YM-254890 (100 nmol/L), or dimethyl sulfoxide (DMSO; vehicle; F) or U-73122 (10 μmol/L), Y-27632 (10 μmol/L), or DMSO (vehicle; I). G, H, J, and K, Percentage of maximal (max.) decrease in norm. resistance (G and J) and of recovery of norm. resistance (H and K) in response to Thr. application as shown in F and I. Data are shown as mean±SD (B, E, G, H, J, and K), and P values were determined by 2-way ANOVA followed by Sidak multiple comparison tests (B), 1-way ANOVA followed by Tukey multiple comparison tests (E), and unpaired 2-tailed Student t test (G, H, J, and K).

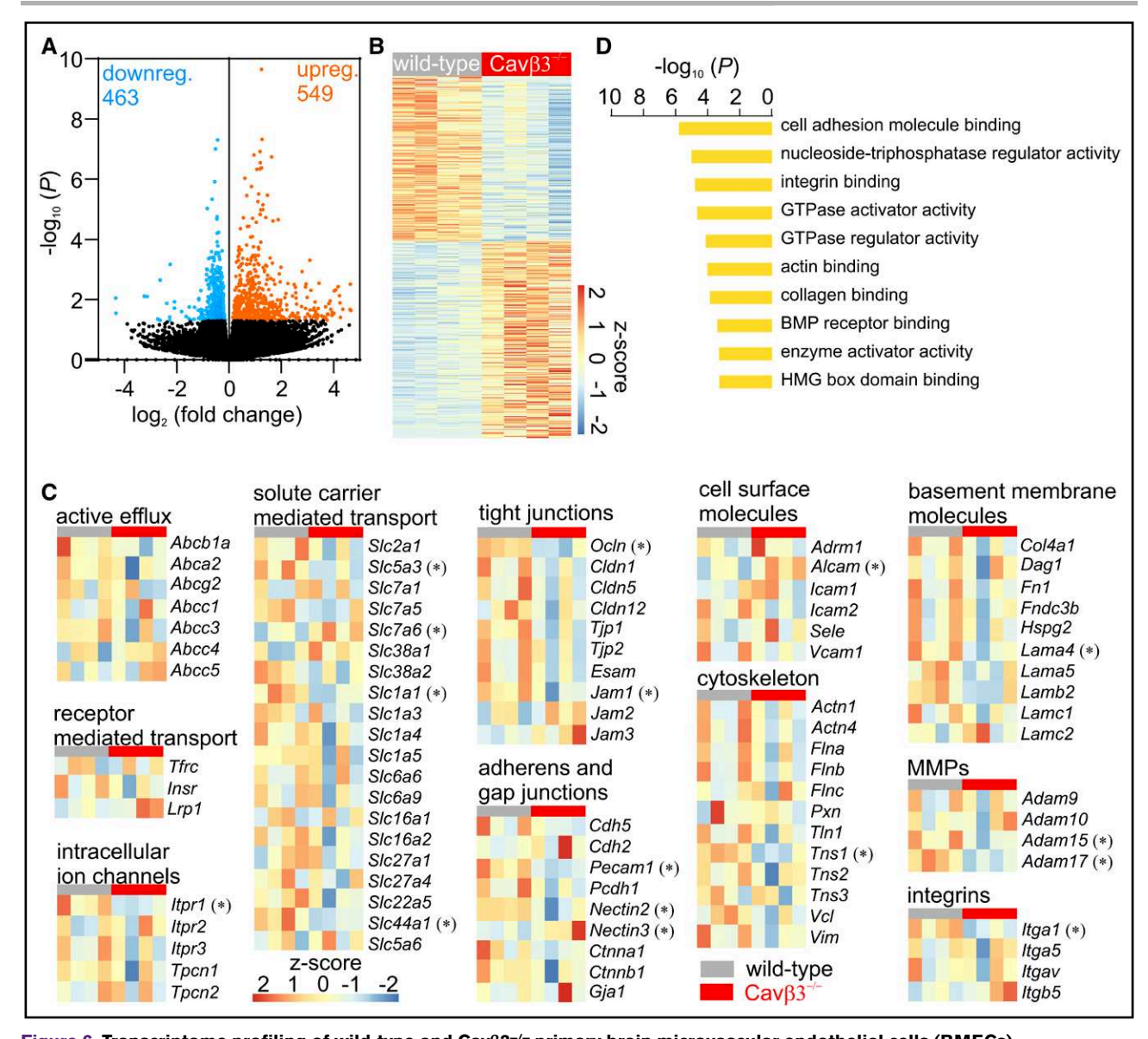


Figure 6. Transcriptome profiling of wild-type and Cavβ3<sup>-/-</sup> primary brain microvascular endothelial cells (BMECs). **A**, Volcano plots illustrating genes differentially expressed between wild-type and  $Cavβ3^{-/-}$  BMECs identified by RNA-seq. Unchanged (black), upregulated (upreg.; orange), and downregulated (downreg.; blue) genes are shown. **B**, Heatmap of expression values illustrating differentially expressed genes (shown in **A**) from 4 independent primary BMEC preparations. **C**, Heatmaps illustrating genes involved in active efflux, receptor-mediated transport, intracellular ion channels, solute carrier-mediated transport, tight junctions, adherens and gap junctions, cell surface molecules, cytoskeleton, basal membrane molecules, MMP (matrix metalloproteinase), and integrins. In **B** and **C**, the scale bar indicates row *Z* scores of gene expression (fragments per kilobase of transcript per million mapped reads) values. Highly expressed genes are shown in red, and genes with low expression are shown in blue. **D**, Gene ontology (GO) terms for molecular processes of genes modulated in  $Cavβ3^{-/-}$  BMECs, with the enrichment score ( $-log_{10}[P]$ ). \*Genes significantly (P<0.05) changed between both genotypes. BMP indicates bone morphogenetic protein; and HMG, high mobility group.

associated with the Cav $\beta$ 3 protein.  $^{61,64}$  Among the Cav $\beta$ 3-associated proteins were the large-conductance Ca<sup>2+</sup> and voltage-activated K<sup>+</sup> channel (KCa1.1) protein,  $^{66}$  syntaxin, and SNAP-25<sup>67</sup> that have been also shown to interact directly with Cav channel subunits (Figure 4G; Table S1). N-cadherin, which is present in endothelial cells and supports their interaction with surrounding pericytes,  $^{68,69}$  was among the proteins associated with Cav $\beta$ 3 in the brain (Table S1). Deletion of the N-cadherin gene *cdh*2 in endothelial cells significantly

increased vascular permeability and resulted in severe vascularization defects leading to embryonic lethality.  $^{70,71}$  The N-cadherin–Cav $\beta3$  interaction may also contribute to the stabilization of microvascular barrier function in the brain.

Cytoplasmic  $Ca^{2+}$  has been shown to affect the permeability of endothelial monolayers since pretreatment with the  $Ca^{2+}$  chelator BAPTA-AM decreases the basal permeability of endothelial monolayers,<sup>8</sup> whereas in the absence of  $Cav\beta 3$ , the basal cytoplasmic  $Ca^{2+}$  concentration of

unstimulated BMECs is slightly but significantly increased (Figure 4A and 4B; Figure S4A and S4B). At the same time, Cav $\beta$ 3-/- BMECs reveal reduced cell area and normalized tight junction length (Figure 3G and 3J). In the presence of the proinflammatory mediator thrombin,  $^{2,72}$  the cytoplasmic Ca<sup>2+</sup> concentration is increased in Cav $\beta$ 3-/- BMECs (Figure 4A and 4B) and the transendothelial resistance of BMEC monolayers is reduced to a greater extent in the absence of Cav $\beta$ 3 (Figure 3A and 3B). These effects on Ca<sup>2+</sup> signaling and permeability of the endothelial barrier were rescued by overexpressing the *Cacnb3* cDNA in Cav $\beta$ 3-/- BMECs and bEnd.3 cells (Figure 3C, 3D, 4C, and 4D; Figure S3A through S3D).

Thrombin increases the permeability of the endothelial barrier by acting on PAR-1 receptors coupled to the G proteins  $G\alpha_{q/11}$  and  $G\alpha_{12/13}$ , thereby increasing IP3 generation and RhoA activity in endothelial cells.  $^{72.73}$  In Cav $\beta$ 3 $^{-/-}$  BMECs, thrombin-induced Ca $^{2+}$  release and MLC phosphorylation were significantly increased compared with wild-type cells (Figures 4A, 4B, 5A, and 5B), whereas basal and thrombin-induced IP3 formation (Figure 4E), Ca $^{2+}$  content of intracellular stores, and storeactivated Ca $^{2+}$  entry were not different in BMECs of both genotypes (Figure S4A through S4C).

The thrombin-induced decrease in transendothelial resistance was more pronounced in the absence of Cavβ3 than in the presence of Cavβ3 (Figure 3A and 3B). Pretreatment of the cells with the MLCK inhibitor ML-7 abolished this difference, as did preincubation with the PLC inhibitor U-73122 or the  $G\alpha_{\alpha/11}$  inhibitor YM-254890 (Figure 5F through 5K). In contrast, after preincubation of BMECs in the presence of the Rho kinase inhibitor Y-27632, the thrombin-induced decrease in transendothelial resistance remained more pronounced in the absence of CavB3 than in the presence of Cavβ3 (Figure 5I through 5K). These data indicate that Cavβ3 modulates the activity of the MLCK indirectly by fine tuning the cytoplasmic Ca2+ in endothelial cells. In the absence of Cavβ3, IP3-dependent Ca<sup>2+</sup> release from intracellular stores is increased, leading to enhanced Ca<sup>2+</sup>-dependent phosphorylation of MLCs by MLCK, followed by their interaction with the actin cytoskeleton, endothelial cell contraction, disrupted tight junctions, and reduced cell area.7,8 Genetic ablation of the PAR-1 receptor significantly attenuated thrombinmediated endothelial hyperpermeability and phosphorylation of MLCs.3 Endothelial permeability was shown to require  $G\alpha_{\alpha/11}$ -mediated signaling in endothelial cells but not  $G\alpha_{19/13}$ . Vascular permeability under basal conditions and in response to the activation of PAR-1 receptor was severely reduced in mice lacking  $G\alpha_{_{\alpha/11}}$  in endothelial cells but not in mice lacking  $G\alpha_{12/13}$  in endothelial cells.<sup>74</sup>

To gain further insight into the role of  $Cav\beta 3$  in the regulation of  $Ca^{2+}$  signaling and endothelial barrier function, we compared the transcriptome profile of wild-type and  $Cav\beta 3^{-/-}$  BMECs and identified changes in

the expression of genes involved in endothelial barrier function (Figure 6). In Pecam-1 (CD31) knockout mice, the onset of clinical symptoms after induction of EAE was significantly earlier than in control mice, and transendothelial migration of T cells was also increased, indicating a compromised blood-brain barrier.59 Downregulation of ZO-1, encoded by the Tip1 gene, affected the organization of tight junction proteins and increased endothelial cell permeability, suggesting a critical role in maintaining the integrity of endothelial barrier function.75 We identified reduced levels of Pecam-1 (wild-type,  $358.05\pm27.44$ ; Cav $\beta3^{-/-}$ , 290.20 $\pm10.55$ ; P=0.0036) and a slight but not significant reduction of *Tjp1* (wildtype,  $54.07\pm5.88$ ; Cav $\beta$ 3<sup>-/-</sup>,  $43.94\pm6.28$ ; P=0.0566) transcripts in Cavβ3<sup>-/-</sup> BMECs, which may have an additional impact on blood-brain barrier permeability. Deletion of Alcam in mice resulted in increased blood-brain barrier permeability and more pronounced clinical disability after induction of EAE.58 In Cavβ3<sup>-/-</sup> BMECs, Alcam transcript levels were increased (Figure 6C; Table S2), possibly to counteract the increased permeability of the endothelial barrier. Taken together, these results demonstrate that Cavβ3 protein contributes to the integrity of BMEC monolayers in vitro and to the integrity of the blood-brain barrier in vivo, with a significant impact on the severity of clinical EAE disease.

#### **ARTICLE INFORMATION**

Received April 23, 2024; accepted June 21, 2024.

#### **Affiliations**

Experimentelle und Klinische Pharmakologie und Toxikologie, Präklinisches Zentrum für Molekulare Signalverarbeitung, PharmaScienceHub (D.M., S.M.-G., N.K., B.W., C.F.-T., M.R.M., A. Beck, V.F., A. Belkacemi) and Institut für Anatomie und Zellbiologie (F.S.), Universität des Saarlandes, Homburg, Germany. Neurologische Klinik, Universitätsklinikum Heidelberg, Germany (S.K.W., K.P., R.F., R.D.). Clinical Cooperation Unit Neuroncology, German Cancer Consortium (DKTK), German Cancer Research Center (DKFZ), Heidelberg, Germany (R.F., S.K.W.). Now with Pharmakologisches Institut, Ruprecht-Karls-Universität Heidelberg, Germany (A. Belkacemi).

#### **Acknowledgments**

The authors thank Dr Petra Weissgerber and all members of the Transgene Unit of the SPF animal facility of the Medical Faculty, Homburg, for taking care of the animals and the members of the Flockerzi Laboratory Oliver Glaser, Stefanie Buchholz, Christine Wesely, and Martin Simon-Thomas for their excellent technical assistance.

#### Sources of Funding

This study was funded by the Deutsche Forschungsgemeinschaft Research Unit 2289 to V. Flockerzi (FL 153/10-1; FL 153/10-2), R. Diem (Di 935/12-2), F. Schmitz (SCHM 797/7-2), S.K. Williams (FA 1641/2-2); Collaborative Research Center 894 (project identifier: 157660137, sub-project A3) to A. Belkacemi, (sub-project A14) to A. Beck, FE 629/2-1 to C. Fecher-Trost, and INST 256/551-1 FUGB to M.R. Meyer.

#### **Disclosures**

None.

#### Supplemental Material

Supplemental Methods Figures S1-S6 Tables S1 and S2 Major Resources Table

#### **REFERENCES**

- Becker LM, Chen SH, Rodor J, de Rooij L, Baker AH, Carmeliet P. Deciphering endothelial heterogeneity in health and disease at single cell resolution: progress and perspectives. *Cardiovasc Res.* 2023;119:6–27. doi: 10.1093/cvr/cvac018
- Mehta D, Malik AB. Signaling mechanisms regulating endothelial permeability. Physiol Rev. 2006;86:279–367. doi: 10.1152/physrev.00012.2005
- Vogel SM, Gao X, Mehta D, Ye RD, John TA, Andrade-Gordon P, Tiruppathi C, Malik AB. Abrogation of thrombin-induced increase in pulmonary microvascular permeability in PAR-1 knockout mice. *Physiol Genomics*. 2000;4:137– 145. doi: 10.1152/physiolgenomics.2000.4.2.137
- Fasolato C, Nilius B. Store depletion triggers the calcium release-activated calcium current (ICRAC) in macrovascular endothelial cells: a comparison with Jurkat and embryonic kidney cell lines. *Pflugers Arch.* 1998;436:69– 74. doi: 10.1007/s004240050605
- Nilius B, Droogmans G. Ion channels and their functional role in vascular endothelium. *Physiol Rev.* 2001;81:1415–1459. doi: 10.1152/physrev.2001.81.4.1415
- Tiruppathi C, Freichel M, Vogel SM, Paria BC, Mehta D, Flockerzi V, Malik AB. Impairment of store-operated Ca<sup>2+</sup> entry in TRPC4(-/-) mice interferes with increase in lung microvascular permeability. *Circ Res.* 2002;91:70–76. doi: 10.1161/01.res.0000023391.40106.a8
- Dalal PJ, Muller WA, Sullivan DP. Endothelial cell calcium signaling during barrier function and inflammation. Am J Pathol. 2020;190:535–542. doi: 10.1016/j.ajpath.2019.11.004
- van Nieuw Amerongen GP, Draijer R, Vermeer MA, van Hinsbergh VW. Transient and prolonged increase in endothelial permeability induced by histamine and thrombin: role of protein kinases, calcium, and RhoA. Circ Res. 1998;83:1115–1123. doi: 10.1161/01.res.83.11.1115
- Bossu JL, Elhamdani A, Feltz A, Tanzi F, Aunis D, Thierse D. Voltage-gated Ca entry in isolated bovine capillary endothelial cells: evidence of a new type of BAY K 8644-sensitive channel. *Pflugers Arch.* 1992;420:200–207. doi: 10.1007/BF00374991
- Vinet R, Vargas FF. L- and T-type voltage-gated Ca<sup>2+</sup> currents in adrenal medulla endothelial cells. Am J Physiol. 1999;276:H1313-H1322. doi: 10.1152/ajpheart.1999.276.4.H1313
- Catterall WA. Structure and regulation of voltage-gated Ca<sup>2+</sup> channels. Annu Rev Cell Dev Biol. 2000;16:521–555. doi: 10.1146/annurev.cellbio.16.1.521
- Hofmann F, Flockerzi V, Kahl S, Wegener JW. L-type CaV1.2 calcium channels: from in vitro findings to in vivo function. *Physiol Rev.* 2014;94:303–326. doi: 10.1152/physrev.00016.2013
- Wu J, Yan Z, Li Z, Qian X, Lu S, Dong M, Zhou Q, Yan N. Structure of the voltage-gated calcium channel Ca(v)1.1 at 3.6 A resolution. *Nature*. 2016;537:191–196. doi: 10.1038/nature19321
- Dolphin AC. Calcium channel auxiliary alpha2delta and beta subunits: trafficking and one step beyond. Nat Rev Neurosci. 2012;13:542–555. doi: 10.1038/nrn3311
- He LL, Zhang Y, Chen YH, Yamada Y, Yang J. Functional modularity of the beta-subunit of voltage-gated Ca<sup>2+</sup> channels. *Biophys J.* 2007;93:834–845. doi: 10.1529/biophysj.106.101691
- Kadurin I, Ferron L, Rothwell SW, Meyer JO, Douglas LR, Bauer CS, Lana B, Margas W, Alexopoulos O, Nieto-Rostro M, et al. Proteolytic maturation of alpha(2)delta represents a checkpoint for activation and neuronal trafficking of latent calcium channels. *Elife.* 2016;5:e21143. doi: 10.7554/eLife.21143
- Singer D, Biel M, Lotan I, Flockerzi V, Hofmann F, Dascal N. The roles of the subunits in the function of the calcium channel. *Science*. 1991;253:1553– 1557. doi: 10.1126/science.1716787
- Eroglu C, Allen NJ, Susman MW, O'Rourke NA, Park CY, Ozkan E, Chakraborty C, Mulinyawe SB, Annis DS, Huberman AD, et al. Gabapentin receptor alpha2delta-1 is a neuronal thrombospondin receptor responsible for excitatory CNS synaptogenesis. *Cell.* 2009;139:380–392. doi: 10.1016/j.cell.2009.09.025
- Gee NS, Brown JP, Dissanayake VU, Offord J, Thurlow R, Woodruff GN. The novel anticonvulsant drug, gabapentin (Neurontin), binds to the alpha2delta subunit of a calcium channel. *J Biol Chem.* 1996;271:5768–5776. doi: 10.1074/jbc.271.10.5768
- Fell B, Eckrich S, Blum K, Eckrich T, Hecker D, Obermair GJ, Munkner S, Flockerzi V, Schick B, Engel J. alpha2delta2 controls the function and trans-synaptic coupling of Cav1.3 channels in mouse inner hair cells and is essential for normal hearing. J Neurosci. 2016;36:11024– 11036. doi: 10.1523/JNEUROSCI.3468-14.2016
- Schopf CL, Ablinger C, Geisler SM, Stanika RI, Campiglio M, Kaufmann WA, Nimmervoll B, Schlick B, Brockhaus J, Missler M, et al. Presynaptic alpha2delta

- subunits are key organizers of glutamatergic synapses. *Proc Natl Acad Sci USA*. 2021;118:e1920827118. doi: 10.1073/pnas.1920827118
- Etemad S, Obermair GJ, Bindreither D, Benedetti A, Stanika R, Di Biase V, Burtscher V, Koschak A, Kofler R, Geley S, et al. Differential neuronal targeting of a new and two known calcium channel beta4 subunit splice variants correlates with their regulation of gene expression. *J Neuro-sci.* 2014;34:1446–1461. doi: 10.1523/JNEUROSCI.3935-13.2014
- Tadmouri A, Kiyonaka S, Barbado M, Rousset M, Fablet K, Sawamura S, Bahembera E, Pernet-Gallay K, Arnoult C, Miki T, et al. Cacnb4 directly couples electrical activity to gene expression, a process defective in juvenile epilepsy. EMBO J. 2012;31:3730–3744. doi: 10.1038/emboj.2012.226
- Zhang Y, Yamada Y, Fan M, Bangaru SD, Lin B, Yang J. The beta subunit of voltage-gated Ca<sup>2+</sup> channels interacts with and regulates the activity of a novel isoform of Pax6. *J Biol Chem.* 2010;285:2527-2536. doi: 10.1074/jbc.M109.022236
- Traore M, Gentil C, Benedetto C, Hogrel JY, De la Grange P, Cadot B, Benkhelifa-Ziyyat S, Julien L, Lemaitre M, Ferry A, et al. An embryonic CaVbeta1 isoform promotes muscle mass maintenance via GDF5 signaling in adult mouse. Sci Transl Med. 2019;11:eaaw1131. doi: 10.1126/scitranslmed.aaw1131
- Vergnol A, Traore M, Pietri-Rouxel F, Falcone S. New insights in CaVbeta subunits: role in the regulation of gene expression and cellular homeostasis. Front Cell Dev Biol. 2022;10:880441. doi: 10.3389/fcell.2022.880441
- Pickel S, Cruz-Garcia Y, Bandleon S, Barkovits K, Heindl C, Volker K, Abesser M, Pfeiffer K, Schaaf A, Marcus K, et al. The beta2-subunit of voltage-gated calcium channels regulates cardiomyocyte hypertrophy. Front Cardiovasc Med. 2021;8:704657. doi: 10.3389/fcvm.2021.704657
- Erdogmus S, Concepcion AR, Yamashita M, Sidhu I, Tao AY, Li W, Rocha PP, Huang B, Garippa R, Lee B, et al. Cavbeta1 regulates T cell expansion and apoptosis independently of voltage-gated Ca<sup>2+</sup> channel function. *Nat Com-mun.* 2022;13:2033. doi: 10.1038/s41467-022-29725-3
- Becker A, Wardas B, Salah H, Amini M, Fecher-Trost C, Sen Q, Martus D, Beck A, Philipp SE, Flockerzi V, et al. Cavbeta3 regulates Ca<sup>2+</sup> signaling and insulin expression in pancreatic beta-cells in a cell-autonomous manner. *Diabetes*. 2021;70:2532–2544. doi: 10.2337/db21-0078
- Belkacemi A, Beck A, Wardas B, Weissgerber P, Flockerzi V. IP3-dependent Ca<sup>2+</sup> signals are tightly controlled by Cavβ3, but not by Cavβ1, 2 and 4. *Cell Calcium*. 2022;104:102573. doi: 10.1016/j.ceca.2022.102573
- Belkacemi A, Hui X, Wardas B, Laschke MW, Wissenbach U, Menger MD, Lipp P, Beck A, Flockerzi V. IP3 receptor-dependent cytoplasmic Ca<sup>2+</sup> signals are tightly controlled by Cavbeta3. *Cell Rep.* 2018;22:1339–1349. doi: 10.1016/j.celrep.2018.01.010
- Belkacemi A, Laschke MW, Menger MD, Flockerzi V. Scratch migration assay and dorsal skinfold chamber for in vitro and in vivo analysis of wound healing. J Vis Exp. 2019:(151). doi: 10.3791/59608
- Berggren PO, Yang SN, Murakami M, Efanov AM, Uhles S, Kohler M, Moede T, Fernstrom A, Appelskog IB, Aspinwall CA, et al. Removal of Ca<sup>2+</sup> channel beta3 subunit enhances Ca<sup>2+</sup> oscillation frequency and insulin exocytosis. *Cell.* 2004;119:273–284. doi: 10.1016/j.cell.2004.09.033
- Perez-Riverol Y, Bai J, Bandla C, Garcia-Seisdedos D, Hewapathirana S, Kamatchinathan S, Kundu DJ, Prakash A, Frericks-Zipper A, Eisenacher M, et al. The PRIDE database resources in 2022: a hub for mass spectrometrybased proteomics evidences. *Nucleic Acids Res.* 2022;50:D543–D552. doi: 10.1093/nar/gkab1038
- Ryan L, Mills KHG. Sex differences regulate immune responses in experimental autoimmune encephalomyelitis and multiple sclerosis. Eur J Immunol. 2022;52:24–33. doi: 10.1002/eji.202149589
- Constantinescu CS, Farooqi N, O'Brien K, Gran B. Experimental autoimmune encephalomyelitis (EAE) as a model for multiple sclerosis (MS). *Br J Phar-macol.* 2011;164:1079–1106. doi: 10.1111/j.1476-5381.2011.01302.x
- Kollewe A, Schwarz Y, Oleinikov K, Raza A, Haupt A, Wartenberg P, Wyatt A, Boehm U, Ectors F, Bildl W, et al. Subunit composition, molecular environment, and activation of native TRPC channels encoded by their interactomes. Neuron. 2022;110:4162–4175.e7. doi: 10.1016/j.neuron.2022.09.029
- Williams SK, Fairless R, Maier O, Liermann PC, Pichi K, Fischer R, Eisel ULM, Kontermann R, Herrmann A, Weksler B, et al. Anti-TNFR1 targeting in humanized mice ameliorates disease in a model of multiple sclerosis. Sci Rep. 2018;8:13628. doi: 10.1038/s41598-018-31957-7
- Schindelin J, Arganda-Carreras I, Frise E, Kaynig V, Longair M, Pietzsch T, Preibisch S, Rueden C, Saalfeld S, Schmid B, et al. Fiji: an open-source platform for biological-image analysis. *Nat Methods*. 2012;9:676–682. doi: 10.1038/nmeth.2019
- Ruck T, Bittner S, Epping L, Herrmann AM, Meuth SG. Isolation of primary murine brain microvascular endothelial cells. J Vis Exp. 2014;93:e52204. doi: 10.3791/52204

- 41. Belkacemi A, Trost CF, Tinschert R, Flormann D, Malihpour M, Wagner C, Meyer MR, Beck A, Flockerzi V. The TRPV2 channel mediates Ca<sup>2+</sup> influx and the Delta9-THC-dependent decrease in osmotic fragility in red blood cells. *Haematologica*. 2021;106:2246–2250. doi: 10.3324/haematol.2020.274951
- Fecher-Trost C, Wissenbach U, Beck A, Schalkowsky P, Stoerger C, Doerr J, Dembek A, Simon-Thomas M, Weber A, Wollenberg P, et al. The in vivo TRPV6 protein starts at a non-AUG triplet, decoded as methionine, upstream of canonical initiation at AUG. *J Biol Chem.* 2013;288:16629– 16644. doi: 10.1074/jbc.M113.469726
- Xiao C, Lachance B, Sunahara G, Luong JH. An in-depth analysis of electric cell-substrate impedance sensing to study the attachment and spreading of mammalian cells. *Anal Chem.* 2002;74:1333–1339. doi: 10.1021/ac011104a
- McMillin MA, Frampton GA, Seiwell AP, Patel NS, Jacobs AN, DeMorrow S. TGFbeta1 exacerbates blood-brain barrier permeability in a mouse model of hepatic encephalopathy via upregulation of MMP9 and downregulation of claudin-5. *Lab Invest*. 2015;95:903–913. doi: 10.1038/labinvest.2015.70
- Fairless R, Williams SK, Hoffmann DB, Stojic A, Hochmeister S, Schmitz F, Storch MK, Diem R. Preclinical retinal neurodegeneration in a model of multiple sclerosis. *J Neurosci.* 2012;32:5585–5597. doi: 10.1523/JNEUROSCI.5705-11.2012
- Cory AH, Owen TC, Barltrop JA, Cory JG. Use of an aqueous soluble tetrazolium/formazan assay for cell growth assays in culture. *Cancer Commun*. 1991;3:207–212. doi: 10.3727/095535491820873191
- Woo MS, Ufer F, Sonner JK, Belkacemi A, Tintelnot J, Saez PJ, Krieg PF, Mayer C, Binkle-Ladisch L, Engler JB, et al. Calcium channel beta3 subunit regulates ATP-dependent migration of dendritic cells. Sci Adv. 2023;9:eadh1653. doi: 10.1126/sciadv.adh1653
- Wen S, Gotze IN, Mai O, Schauer C, Leinders-Zufall T, Boehm U. Genetic identification of GnRH receptor neurons: a new model for studying neural circuits underlying reproductive physiology in the mouse brain. *Endocrinology*. 2011;152:1515–1526. doi: 10.1210/en.2010-1208
- Perriere N, Demeuse P, Garcia E, Regina A, Debray M, Andreux JP, Couvreur P, Scherrmann JM, Temsamani J, Couraud PO, et al. Puromycinbased purification of rat brain capillary endothelial cell cultures. Effect on the expression of blood-brain barrier-specific properties. *J Neurochem*. 2005;93:279–289. doi: 10.1111/j.1471-4159.2004.03020.x
- Song HW, Foreman KL, Gastfriend BD, Kuo JS, Palecek SP, Shusta EV. Transcriptomic comparison of human and mouse brain microvessels. Sci Rep. 2020;10:12358. doi: 10.1038/s41598-020-69096-7
- McKenzie AT, Wang M, Hauberg ME, Fullard JF, Kozlenkov A, Keenan A, Hurd YL, Dracheva S, Casaccia P, Roussos P, et al. Brain cell type specific gene expression and co-expression network architectures. *Sci Rep.* 2018;8:8868. doi: 10.1038/s41598-018-27293-5
- Darmanis S, Sloan SA, Zhang Y, Enge M, Caneda C, Shuer LM, Hayden Gephart MG, Barres BA, Quake SR. A survey of human brain transcriptome diversity at the single cell level. *Proc Natl Acad Sci USA*. 2015;112:7285-7290. doi: 10.1073/pnas.1507125112
- Muller AM, Hermanns MI, Skrzynski C, Nesslinger M, Muller KM, Kirkpatrick CJ. Expression of the endothelial markers PECAM-1, vWf, and CD34 in vivo and in vitro. Exp Mol Pathol. 2002;72:221–229. doi: 10.1006/exmp.2002.2424
- Ohtsuki S, Yamaguchi H, Katsukura Y, Asashima T, Terasaki T. mRNA expression levels of tight junction protein genes in mouse brain capillary endothelial cells highly purified by magnetic cell sorting. *J Neurochem*. 2008;104:147–154. doi: 10.1111/j.1471-4159.2007.05008.x
- 55. van Nieuw Amerongen GP, van Delft S, Vermeer MA, Collard JG, van Hinsbergh VW. Activation of RhoA by thrombin in endothelial hyper-permeability: role of Rho kinase and protein tyrosine kinases. *Circ Res.* 2000;87:335–340. doi: 10.1161/01.res.87.4.335
- Bkaily G, d'Orleans-Juste P, Naik R, Perodin J, Stankova J, Abdulnour E, Rola-Pleszczynski M. PAF activation of a voltage-gated R-type Ca<sup>2+</sup> channel in human and canine aortic endothelial cells. *Br J Pharmacol.* 1993;110:519– 520. doi: 10.1111/j.1476-5381.1993.tb13841.x
- 57. Stone LA, Smith ME, Albert PS, Bash CN, Maloni H, Frank JA, McFarland HF. Blood-brain barrier disruption on contrast-enhanced MRI in patients with mild relapsing-remitting multiple sclerosis: relationship to course, gender, and age. Neurology. 1995;45:1122–1126. doi: 10.1212/wnl.45.6.1122

- Lecuyer MA, Saint-Laurent O, Bourbonniere L, Larouche S, Larochelle C, Michel L, Charabati M, Abadier M, Zandee S, Haghayegh Jahromi N, et al. Dual role of ALCAM in neuroinflammation and blood-brain barrier homeostasis. *Proc Natl Acad Sci USA*. 2017;114:E524–E533. doi: 10.1073/pnas.1614336114
- Graesser D, Solowiej A, Bruckner M, Osterweil E, Juedes A, Davis S, Ruddle NH, Engelhardt B, Madri JA. Altered vascular permeability and early onset of experimental autoimmune encephalomyelitis in PECAM-1-deficient mice. *J Clin Invest.* 2002;109:383–392. doi: 10.1172/JCI13595
- Ludwig A, Flockerzi V, Hofmann F. Regional expression and cellular localization of the alpha1 and beta subunit of high voltage-activated calcium channels in rat brain. *J Neurosci.* 1997;17:1339–1349. doi: 10.1523/JNEUROSCI.17-04-01339.1997
- Muller CS, Haupt A, Bildl W, Schindler J, Knaus HG, Meissner M, Rammner B, Striessnig J, Flockerzi V, Fakler B, et al. Quantitative proteomics of the Cav2 channel nano-environments in the mammalian brain. *Proc Natl Acad Sci* USA. 2010;107:14950–14957. doi: 10.1073/pnas.1005940107
- Murakami M, Fleischmann B, De Felipe C, Freichel M, Trost C, Ludwig A, Wissenbach U, Schwegler H, Hofmann F, Hescheler J, et al. Pain perception in mice lacking the beta3 subunit of voltage-activated calcium channels. *J Biol Chem.* 2002;277:40342–40351. doi: 10.1074/jbc.M203425200
- Namkung Y, Smith SM, Lee SB, Skrypnyk NV, Kim HL, Chin H, Scheller RH, Tsien RW, Shin HS. Targeted disruption of the Ca<sup>2+</sup> channel beta3 subunit reduces N- and L-type Ca<sup>2+</sup> channel activity and alters the voltagedependent activation of P/Q-type Ca<sup>2+</sup> channels in neurons. *Proc Natl Acad Sci USA*. 1998;95:12010–12015. doi: 10.1073/pnas.95.20.12010
- Scott VE, De Waard M, Liu H, Gurnett CA, Venzke DP, Lennon VA, Campbell KP. Beta subunit heterogeneity in N-type Ca<sup>2+</sup> channels. *J Biol Chem.* 1996;271:3207–3212. doi: 10.1074/jbc.271.6.3207
- Tokuhara N, Namiki K, Uesugi M, Miyamoto C, Ohgoh M, Ido K, Yoshinaga T, Yamauchi T, Kuromitsu J, Kimura S, et al. N-type calcium channel in the pathogenesis of experimental autoimmune encephalomyelitis. *J Biol Chem.* 2010;285:33294–33306. doi: 10.1074/jbc.M109.089805
- Berkefeld H, Sailer CA, Bildl W, Rohde V, Thumfart JO, Eble S, Klugbauer N, Reisinger E, Bischofberger J, Oliver D, et al. BKCa-Cav channel complexes mediate rapid and localized Ca<sup>2+</sup>-activated K+ signaling. Science. 2006;314:615–620. doi: 10.1126/science.1132915
- 67. Rettig J, Sheng ZH, Kim DK, Hodson CD, Snutch TP, Catterall WA. Isoform-specific interaction of the alpha1A subunits of brain Ca<sup>2+</sup> channels with the presynaptic proteins syntaxin and SNAP-25. *Proc Natl Acad Sci USA* 1996;93:7363–7368. doi: 10.1073/pnas.93.14.7363
- Navarro P, Ruco L, Dejana E. Differential localization of VE- and N-cadherins in human endothelial cells: VE-cadherin competes with N-cadherin for junctional localization. *J Cell Biol.* 1998;140:1475–1484. doi: 10.1083/jcb.140.6.1475
- Salomon D, Ayalon O, Patel-King R, Hynes RO, Geiger B. Extrajunctional distribution of N-cadherin in cultured human endothelial cells. *J Cell Sci*. 1992;102(pt 1):7–17. doi: 10.1242/jcs.102.1.7
- Kruse K, Lee QS, Sun Y, Klomp J, Yang X, Huang F, Sun MY, Zhao S, Hong Z, Vogel SM, et al. N-cadherin signaling via Trio assembles adherens junctions to restrict endothelial permeability. *J Cell Biol.* 2019;218:299–316. doi: 10.1083/jcb.201802076
- Luo Y, Radice GL. N-cadherin acts upstream of VE-cadherin in controlling vascular morphogenesis. J Cell Biol. 2005;169:29–34. doi: 10.1083/jcb.200411127
- Wettschureck N, Strilic B, Offermanns S. Passing the vascular barrier: endothelial signaling processes controlling extravasation. *Physiol Rev.* 2019;99:1467–1525. doi: 10.1152/physrev.00037.2018
- 73. Coughlin SR. Thrombin signalling and protease-activated receptors. *Nature*. 2000;407:258–264. doi: 10.1038/35025229
- Korhonen H, Fisslthaler B, Moers A, Wirth A, Habermehl D, Wieland T, Schutz G, Wettschureck N, Fleming I, Offermanns S. Anaphylactic shock depends on endothelial Gq/G11. J Exp Med. 2009;206:411–420. doi: 10.1084/jem.20082150
- Diagbouga MR, Morel S, Cayron AF, Haemmerli J, Georges M, Hierck BP, Allemann E, Lemeille S, Bijlenga P, Kwak BR. Primary cilia control endothelial permeability by regulating expression and location of junction proteins. Cardiovasc Res. 2022;118:1583–1596. doi: 10.1093/cvr/cvab165